NASA Technical Paper 1703

Aerothermal Analysis of a Wing-Elevo Cove With Variable Leakage

L. Roane Hunt

SEPTEMBER 1980

NASA

NASA Technical Paper 1703

Aerothermal Analysis of a Wing-Elevon Cove With Variable Leakage

L. Roane Hunt
Langley Research Center
Hampton, Virginia

National Aeronautics
and Space Administration

**Scientific and Technical
Information Branch**

1980

SUMMARY

A mathematical model of the heating associated with leakage within the Space Shuttle Orbiter wing-elevon cove was used to analyze the aerothermal response of the structure. The analysis was applied to wind-tunnel results and to shuttle-entry conditions. Flow in the cove was modeled as developing flow between parallel plates. The mass flow entering the cove was assumed to be the portion of the external-flow boundary layer that is next to the wing surface ahead of the cove. A parametric study described the mechanism by which the energy of the ingested mass is distributed as a function of the Reynolds number, wall conductivity, surface emissivity, and cove height and length. In general, the rate at which energy was transferred into the cove interior was primarily determined by the combined effects of the convection, wall capacitance, and internal-radiation terms.

Correlation with wind-tunnel results indicated that the cold-wall convective heating rates, wall temperature, and gas temperature of the cove were predicted by the analytical model for short exposure times. Predicted transient thermal response of the elevon cove subjected to shuttle-entry conditions indicated that the allowable leak area at the cove seal was 20 percent less than that previously indicated by experiment. To predict more accurate structural temperatures, the techniques used herein to represent the convective heat transfer must be incoporated into a more detailed structural model which would more accurately represent the cove geometry and thermal mass distribution.

INTRODUCTION

Shuttle-type entry vehicles and hypersonic cruise aircraft experience differential pressure across the wings that can promote hot boundary-layer gas ingestion into the wing-elevon cove region as illustrated in figure 1. The cross section of the shuttle wing shows gas leakage through the cove, past a rub seal, and into the interior cavity. Predicted external-surface temperatures at the shuttle wing-elevon junction can be as high as 1280 K (ref. 1). Obviously, the internal structure cannot withstand exposure to ingested gases at such elevated temperatures. Therefore, the gas ingestion must at least be minimized by cove seals such as the rub seal shown in figure 1. Since the design of an absolute seal is improbable, considerable effort has been made to determine the effects of cove leakage.

A number of experimental investigators (refs. 2 to 5) have studied heating trends in the wing-elevon cove region. Experimental pressure and convective cold-wall heating-rate data, obtained by using small wedge-flap models (refs. 2 and 3), indicate that pressure and heating decreased along the cove. Similar heating trends were obtained (ref. 4) from short-time tests (approximately 20 s) by using a full-scale model representing a section of the windward surface of the shuttle at the wing-elevon juncture. However, after an initial decrease at the entrance, the pressure remained constant along the cove up to the flow

restriction representing the seal at the end of the cove. In another experimental investigation (ref. 5), a full-scale model that was geometrically and structurally similar to the shuttle cove was subjected to a simulated shuttle-entry environment (up to 1800 s) to determine the allowable seal gap. The correct thermal mass characteristics were considered important to simulate the hot-wall convective heating conditions and the internal radiation which was assumed to be a major contributor to the heat load of the cove interior. The temperature of the internal structure was monitored during each entry exposure at various seal-gap heights to determine the allowable gap size.

Although the thermal response of a wing-elevon cove has been studied experimentally, a real need exists for adequate analytical tools that can be used to predict cove response under actual flight conditions, and some efforts have been made to meet this need. For example, in reference 6 a detailed flow analysis of ingested gas is presented and the results of calculations are shown to be in reasonably good agreement with the experimental measurements of references 2 and 3 for steady-state pressures and heating rates. In this analysis, the fluid is a perfect gas with constant molecular weight and specific heat; and the one-dimensional flow analysis is combined with flat-plate heating correlations and nonsimilar boundary-layer computer solutions. The mean enthalpy of the ingested flow was obtained by an integration of the external boundary-layer flow.

The present study was initiated to develop a convenient mathematical model that would be useful in predicting the thermal response of a wing-elevon cove during flight. The model described herein incorporates (1) a simplified one-dimensional flow analysis of the gas leaking through the complex cove geometry, and (2) the time-dependent thermal response of the structure. The analysis also accounts for convection from the ingested external boundary-layer gas, conduction along the cove walls, and internal radiation of the cove walls. The validity of the model is established herein by comparison with the experimental results of reference 4 and by the rational trends obtained from a parametric study. The model is then applied to predict the thermal response of the elevon cove to shuttle-entry conditions. The analysis presented herein is based in large part upon the analytical model developed in reference 7.

SYMBOLS

A_c cove area, m^2

A_l cove leak area, m^2

B cove wall thickness, m

c_p specific heat at constant pressure, J/kg-K

D cove gap height, m

D_h cove hydraulic diameter, m

d cove leak-slot height, m

$F(z)$	radiation view factor between cove wall and environment at each end of cove
h	heat-transfer coefficient, W/m^2-K
$K(z)$	radiation view-factor term between cove walls
k	thermal conductivity, W/m-K
L	cove length, m
l	cove leak-slot length, m
$\dot{m}$	mass-flow rate, kg/s
N	number of finite-difference segments
N_{Nu}	Nusselt number
N_{Pr}	Prandtl number
p	pressure, Pa
Δp	differential pressure, Pa
Q	heating rate, W
q	heating rate per unit area, W/m^2
R	free-stream Reynolds number, m^{-1}
R_c	cove Reynolds number, $\frac{\rho V D_h}{\mu}$
T	temperature, K
t	time, s
V	velocity, m/s
x	distance along cove length, m
y	partial boundary-layer thickness (fig. 13), m
z	dummy argument for view-factor equation
α	angle of attack, deg
δ	elevon deflection angle, deg
ϵ	surface emissivity

μ	absolute viscosity, $N\text{-}s/m^2$
ρ	density, kg/m^3
σ	Stefan-Boltzmann constant, $W/m^2\text{-}K^4$
ϕ	distance along cove length of opposite wall, m

Subscripts:

c	convection
env	radiation to cove wall from environment at cove ends
ex	cove-exit value
g	cove-leak gas
i	initial wall value
in	cove-entrance value
k	conduction
m	convective mass transport
max	maximum
o	environment at cove ends
opp	radiation to cove wall from opposite wall
out	radiation from wall
RSI	reusable surface insulation
r	net radiation
rub	rub tube
s	wing surface
sw	stored in wall
w	cove wall
∞	developed channel flow

ANALYSIS

A simplified mathematical model has been developed for determining the aerothermal response of the Space Shuttle Orbiter cove formed at the wing-elevon junction. The ingested gas is assumed to be a perfect gas in equilibrium and the gas properties vary with temperature. The ingested gas flow is assumed to be a one-dimensional, hydraulically and thermally developing flow between two parallel straight plates; the effects of the curved-flow path on convection and radiation are assumed negligible. The flow properties are evaluated locally along the cove. The model is subdivided into a fluid model and a wall model as shown in figure 2.

Fluid Model

The fluid model, illustrated in figure 2(a), includes the convective mass transport of the fluid and the convection between the fluid and the wall surfaces, but the conduction through the fluid and the energy stored in the fluid are both neglected. Laminar flow is assumed with the cove of unit width.

Convective mass transport.- The convective mass transport or net energy transferred along the cove in the flow direction is given by

$$Q_m = Q_{m,in} - Q_{m,ex} = \dot{m} c_{p,g} \frac{\partial T_g(x,t)}{\partial x} dx \tag{1}$$

where

$$\dot{m} = \rho_g V_g D$$

Surface convection.- The surface convection between the fluid and one wall is given by

$$Q_c = h(x,t)\, dx\, [T_g(x,t) - T_w(x,t)] \tag{2}$$

where

$$h(x,t) = N_{Nu}(x,t)\frac{k_g}{D_h}$$

and

$$N_{Nu}(x,t) = N_{Nu,\infty} + \frac{0.036 \dfrac{R_c N_{Pr}}{(x + \delta')/D_h}}{1 + 0.0011 \dfrac{R_c N_{Pr}}{(x + \delta')/D_h}} \tag{3}$$

as obtained from reference 8. The parameter δ' is a number (0.01 for the present analysis) that assures a realistically large value of $N_{Nu}(x,t)$ at the cove entrance rather than an indeterminate value. The symbol $N_{Nu,\infty}$ is the Nusselt number for fully developed flow between uniformly heated parallel plates and has a constant value of 8.23 (ref. 9).

Energy balance.- A first-order differential equation is obtained from the summation of the energy transfer terms defined by equations (1) and (2) and is given by

$$2h(x,t)\left[T_g(x,t) - T_w(x,t)\right] + \rho_g c_{p,g} V_g D \frac{\partial T_g(x,t)}{\partial x} = 0 \tag{4}$$

The coefficient of 2 denotes that two walls exchange heat with the same ingested mass flow. The gas-temperature distribution $T_g(x,t)$ is obtained from the numerical solution of this equation for a given wall-temperature distribution $T_w(x,t)$ and for the boundary condition where the entrance gas temperature $T_g(0,t)$ is specified or computed.

Wall Model

The wall model, illustrated in figure 2(b), includes the conduction along the wall, the net-radiation exchange at the wall surface, and the energy stored in the wall. The convection to the wall is also included and is the same as that used for the fluid model (eq. (2)).

Conduction.- The net conduction across the segment dx, as discussed in reference 10, is given by

$$Q_k = k_w B \frac{\partial^2 T_w(x,t)}{\partial x^2}\, dx \tag{5}$$

Radiation.- The radiation exchange between surfaces was analyzed by neglecting reflected radiation. The radiation leaving the wall surface dx is expressed as

$$Q_{out} = \varepsilon\sigma \, dx \, T_w^4(x,t) \tag{6}$$

The radiation arriving at surface dx from the segments of the opposite wall is expressed as

$$Q_{opp} = \varepsilon\sigma \, dx \int_0^L K(x-\phi) \, T_w^4(\phi,t) \, d\phi \tag{7}$$

where $K(x-\phi) \, d\phi$ is the view factor between segments $d\phi$ and dx and is defined by the following equation based on reference 11:

$$K(z) \, d\phi = \frac{D^2 \, d\phi}{2(D^2 + z^2)^{3/2}} \tag{8}$$

where z is the axial distance between segments ($z = x - \phi$). The radiation arriving at dx from both ends of the cove (or channel) is given by the expression

$$Q_{env} = \varepsilon\sigma \, dx \left[F(x) \, T_o^4(0,t) + F(L-x) \, T_o^4(L,t)\right] \tag{9}$$

where the view factor is defined by the following equation based on reference 11:

$$F(z) = \frac{1}{2} - \frac{z}{2(z^2 + D^2)^{1/2}} \tag{10}$$

The temperatures $T_o(0,t)$ and $T_o(L,t)$ are the physical-boundary temperatures at each end of the cove. For the present analysis, T_o at the entrance was specified as the initial wall value. The T_o at the exit was set equal to the exit wall temperature $T_w(L,t)$. The net-radiation exchange for a wall segment is given by the following sum:

$$Q_r = Q_{out} - Q_{opp} - Q_{env} \tag{11}$$

Energy stored.- The energy stored in a wall segment is given by the following expression:

$$Q_{sw} = \rho_w c_{p,w} B \, dx \, \frac{\partial T_w(x,t)}{\partial t} \tag{12}$$

Energy balance.- Summing the appropriate energy transfer and storage terms and linearizing the radiation term by using the previous time step $t-1$ yield the following expression:

$$h(x,t)\left[T_g(x,t) - T_w(x,t)\right] - k_w B \frac{\partial^2 T_w(x,t)}{\partial x^2} - \varepsilon\sigma\left[T_w^3(x,t-1)\, T_w(x,t) - \int_0^L K(x-\phi)\, T_w^4(\phi,t-1)\, d\phi - F(x)\, T_o^4(0,t-1) - F(L-x)\, T_o^4(L,t-1)\right]$$

$$= \rho_w c_{p,w} B \frac{\partial T_w(x,t)}{\partial t} \tag{13}$$

where the initial wall-temperature distribution $T_w(x,0)$ (designated T_i) is specified and the boundary conditions at $x = 0$ and $x = L$ are, respectively,

$$\frac{\partial T_w(0,t)}{\partial x} = 0$$

and

$$\frac{\partial T_w(L,t)}{\partial x} = 0$$

Values of $T_w(0,t)$ and $T_w(L,t)$ are calculated at each time step by using a finite-difference form of the governing equation and by using terms evaluated at the temperature of the previous time step. The value for $T_w(0,t)$ is calculated by using forward spatial differencing typically shown in reference 10. Thus,

$$h(0,t)\left[T_g(0,t-1) - T_w(0,t-1)\right]$$

$$- \frac{k_w B}{\Delta x^2}\left[T_w(0,t-1) - T_w(\Delta x,t-1)\right]$$

$$- \varepsilon\sigma\left[T_w^4(0,t-1) - \sum_{j=1}^{N} K(0-\phi_j)\, T_w^4(\phi_j,t-1)\, \Delta\phi_j \right.$$

$$\left. - F(0-0)\, T_o^4(0,t-1) - F(0-L)\, T_o^4(L,t-1)\right]$$

$$= \frac{\rho_w c_{p,w} B}{\Delta t}\left[T_w(0,t) - T_w(0,t-1)\right] \tag{14}$$

whereas the value for $T_w(L,t)$ is calculated by using backward spatial differencing (ref. 10):

$$h(L,t)\left[T_g(L,t-1) - T_w(L,t-1)\right]$$

$$- \frac{k_w B}{\Delta x^2}\left[T_w(L-\Delta x,t-1) - T_w(L,t-1)\right]$$

$$- \varepsilon\sigma\left[T_w^4(L,t-1) - \sum_{j=1}^{N} K(L-\phi_j)\, T_w^4(\phi_j,t-1)\, \Delta\phi_j \right.$$

$$\left. - F(L-0)\, T_o^4(0,t-1) - F(L-L)\, T_o^4(L,t-1)\right]$$

$$= \frac{\rho_w c_{p,w} B}{\Delta t}\left[T_w(L,t) - T_w(L,t-1)\right] \tag{15}$$

An iterative process on each time step is used to solve for the gas-temperature distribution $T_g(x,t)$ and the wall-temperature distribution $T_w(x,t)$. At each time step the $T_g(x,t)$ is obtained from equation (4) based on a given $T_w(x,t)$ (either assumed initially or obtained from the previous iteration step). This $T_g(x,t)$ is then used to solve for $T_w(x,t)$ by using

equation (13). The iteration process on each time step is repeated until the values for $T_g(x,t)$ from two successive iterations are within an allowable tolerance.

PARAMETRIC STUDY

Base-Line Conditions

The mathematical model described in the previous section was used to demonstrate and characterize typical results and trends when basic parameters were varied. Selected base-line conditions, many of which are typical of the shuttle-elevon-cove design, were used for this study. The cove wall material was the reusable surface insulation (RSI) and the gas-leakage medium was air. Other base-line values are listed as follows:

Cove height, D, cm	1.27
Cove length, L, cm	38.1
Wall thickness, B, cm	0.64
Wall emissivity, ε	0.8
Entrance gas temperature, $T_g(0,t)$, K	1770
Initial wall temperature, T_i, K	295
Exposure time, t, s	500
Cove Reynolds number, R_c	50
Leakage flow rate, $\dot{m}$, g/s	1.1

Calculated Results for Base-Line Conditions

Typical cove gas- and wall-temperature distributions calculated from the present mathematical model are presented in figure 3 for exposure times from 0 to 500 s. For this example, the gas temperature at the entrance ($x/L = 0$ in fig. 3(a)) was fixed at $T_g(0,t)/T_i = 6$, and the initial wall-temperature distribution ($t = 0$ in fig. 3(b)) was specified at $T_w(x,0)/T_i = 1$. These curves describe a gradual penetration of energy into the cove with exposure time, which is a reasonable expectation. Thus, the initial gas-temperature distribution ($t = 0$ in fig. 3(a)) shows that the finite energy of the ingested gas is transferred to the cold cove walls within the first 30 percent of the cove length, but by $t = 500$ s the gas temperature at the cove exit has increased by a factor of 3. As indicated in figure 3(b), the wall temperature at the cove entrance reached radiation equilibrium first ($t = 100$ s). Then, the interior wall temperature approached equilibrium causing the location of the maximum temperature to move inward. The cooler wall temperature nearest the cove entrance can be explained as an effect of more direct radiation cooling to the external environment. However, convection appears to be the primary factor in control of the wall temperature through most of the cove, since the temperature of the ingested gas was always higher than the wall temperature. The temperature distribution at $t = 500$ s was selected as the base-line condition for this parametric study to represent the total heat load of a shuttle entry. All

examples shown herein include all modes of heat transfer, but parameters which affect individual modes such as cove Reynolds number, thermal conductivity, emissivity, and cove gap height and length were varied to make significant comparisons. The rate at which cove temperatures change is also a function of cove structural mass, but that parameter was not varied.

Effect of Reynolds Numbers

The effect of cove Reynolds number R_c on the calculated cove gas- and wall-temperature distributions at $t = 500$ s is shown in figure 4 for values of R_c from 10 to 1000. As indicated, the cove gas and wall temperatures increased with R_c. This result was expected since R_c is primarily a measure of mass flow in the cove of constant cross-sectional area, and the amount of energy that enters the cove is directly proportional to mass flow when the entrance gas temperature is fixed. Furthermore, the total energy of the ingested mass represents the potential thermal load to the cove interior, and the ingested mass comes from a portion of the external boundary layer next to the wing surface at the cove entrance. Therefore, for constant external-flow conditions, an increase in mass flow into the cove (increased R_c) will also bring an increase in energy content since a greater portion of the external boundary layer containing higher energy flow will be introduced. The results of figure 4 also show that for each R_c the wall-temperature distributions closely follow the gas-temperature distributions except near the cove entrance where direct radiation relief to the external environment caused lower wall temperatures. At $R_c \geq 500$ the calculations yielded gas and wall temperatures throughout most of the cove that were constant and close to the temperature of the gas at the cove entrance. Thus, an equilibrium condition was reached within 500 s at those Reynolds numbers. At lower Reynolds numbers, cove temperatures would also be expected to reach equilibrium but at lower temperature levels and after longer exposure times.

Effect of Wall Thermal Conductivity

The effect of thermal conduction within the cove walls on the calculated cove gas- and wall-temperature distributions is demonstrated in figure 5 for values of $k_w/k_{w,RSI}$ from 0.1 to 1000. The base-line distributions for shuttle RSI are given by the curves for $k_w/k_{w,RSI} = 1$. When k_w was reduced an order of magnitude to $k_w/k_{w,RSI} = 0.1$, the gas- and wall-temperature distributions were unaffected. However, when k_w was increased, the results showed that the cove gas and wall temperatures toward the entrance decreased while these temperatures toward the exit increased. For an increase in k_w by 3 orders of magnitude to $k_w/k_{w,RSI} = 1000$, the cove gas temperature became constant for $x/L \geq 0.3$ and the cove wall temperature was constant over the entire cove length. These results were expected since large increases in k_w allow faster penetration of thermal energy into the cove as energy absorbed by the walls is quickly distributed internally by increased conduction. For the shuttle the cove is constructed of RSI material; therefore, thermal conductivity of the walls should not adversely affect the cove thermal response.

Effect of Surface Emissivity

The effect of surface emissivity on the calculated cove gas- and wall-temperature distributions is illustrated in figure 6 for values of ε from 0 to 1.0. This range of values was chosen to cover the extremes of internal thermal radiation from zero at $\varepsilon = 0$ to maximum at $\varepsilon = 1.0$ where each cove surface absorbs and emits radiation at 100-percent efficiency. Reflected energy was neglected. These results indicate that by decreasing radiation (decreasing ε) there was a corresponding reduction in radiation cooling that allowed the gas and wall temperatures toward the cove entrance to attain progressively higher values. (At $\varepsilon = 0$, the gas and wall temperatures at the entrance are equal.) Also, the gas and wall temperatures toward the cove exit attained progressively lower values as radiation was reduced. Thus, in the example, penetration of energy to the cove interior is retarded by reducing radiation. However, as shown in figure 7, this favorable effect disappears as exposure time increases such that cove exit temperature increases for decreasing radiation. In figure 7, the cove-exit-temperature histories are plotted for various values of ε and over a time period that corresponds to a shuttle entry. These curves show that although reduced radiation is beneficial initially in retarding temperature rise in the cove interior, increased radiation becomes advantageous in promoting radiation cooling during the latter part of the exposure when cove wall temperatures are high. The period of time over which radiation is beneficial would shorten for higher cove Reynolds number because less exposure time would be required to elevate the cove interior temperature. Therefore, the present analysis indicates that thermal radiation is an important factor in transferring energy from the ingested gas to the cove interior during a shuttle entry. A similar conclusion is indicated by some earlier investigations. (See ref. 5.)

Effect of Cove Height and Length

The effect of varying the cove gap height D between the elevon and wing (fig. 2) on the calculated cove gas- and wall-temperature distributions is shown in figure 8. These results show that as cove gap height is reduced with the leakage rate constant, the cove gas and wall temperatures increase toward the entrance and decrease toward the exit in a fashion similar to that shown when the surface emissivity was varied. (See fig. 6.) As indicated by equation (3), reducing cove gap height yields higher heat-transfer coefficients. Consequently, a greater portion of the energy of the ingested gas is absorbed by the cove walls near the entrance as the cove height is reduced. The similarity of trends of these results to those of figure 6 suggest that transfer of energy by radiation to the cove interior also diminishes with decreasing cove gap height. However, as occurred with the effect of surface emissivity discussed in the previous section, this favorable effect disappears and reverses as exposure time increases.

The effect of varying the cove length L (fig. 2) on calculated gas- and wall-temperature responses with time at the cove exit as shown in figure 9 for cove lengths from 12.7 to 76.2 cm. Base-line length is 38.1 cm. These results show that the gas and wall temperatures at the cove exit decrease as cove length is increased. Although slightly lower heat-transfer coefficients are obtained

in the present analysis (eq. (3)) when cove length is increased, the primary factor responsible for the lower exit temperatures is the increase in thermal capacitance of the cove wall that accompanies an increase in cove length. Consequently, longer exposure times are required for penetration of ingested hot gas to the cove interior in coves with greater thermal capacitance.

Summary of Parametric Study

From the results of the parametric study it is seen that the model is able to account for the various modes of heat transfer and to delineate the mechanism by which the energy of the ingested mass is distributed as a function of all these modes. Thus, the present analysis shows that the rate at which energy is transferred to the cove interior primarily depends on convection, wall conduction, internal radiation, and wall thermal capacitance. Although convection controls the cove wall temperature, energy penetration toward the cove exit can be retarded by low wall thermal conductivity, low internal radiation, and high thermal capacitance. However, when cove interior temperatures are high, radiation cools the cove interior.

CORRELATION WITH TEST RESULTS

The present mathematical model was used to analyze the results from aerothermal tests of a large-scale model of a wing-elevon cove shown in figure 10 and described in detail in reference 4. The test model was designed to obtain gas temperatures, pressures, and cold-wall heat-transfer rates within the cove, and, hence, exposure times were short. The general instrumentation distribution is given in figure 11. Tests were made with a turbulent boundary layer on the wing pitched to an angle of attack of 12° and an elevon deflection angle of 10°. The free-stream Mach number was 6.9, the free-stream Reynolds number was 4.4×10^{6} per meter, and the total temperature was 1888 K. Cove leakage was controlled by varying the size of a slot in the seal located at the exit of the cove. The leakage slot was either full or partial span as illustrated in figure 12. The table inset indicates the range of slot dimensions included in this analysis.

Entrance Gas Temperature

For proper correlation with the test results, the cove-entrance boundary conditions were modeled as described in figure 13. In figure 13(a) an illustration of a simplified mathematical model of the present analysis represents the entrance boundary conditions including the ingested mass-flow rate $\dot{m}$ and the gas temperature T_g entering the cove. These entrance conditions are dependent upon the boundary-layer flow ahead of the cove and the external-wing surface temperature T_s. The variation of T_s as a function of time was computed by using wind-tunnel calibration data and the lumped-parameter computer code described in reference 12. Next, the relationship between T_g and $\dot{m}$ was established for several values of T_s by using a nonsimilar, integral method, boundary-layer analysis (ref. 13) of the external flow. The $\dot{m}$ within the cove was assumed to come from the portion of the external boundary layer of thickness

y (fig. 13(b)) next to the wing surface with no mixing at the cove entrance. The mass-related average temperature of the portion of the boundary layer next to the wing surface, which is greatly influenced by T_s, was used as the ingested gas temperature at the cove entrance (fig. 13(c)). The entrance gas temperature, therefore, was a function of T_s and $\dot{m}$ of the ingested flow as presented in figure 14.

The solution used in the present analysis for correlating wind-tunnel test results incorporated iterative procedures that varied the entrance T_g and $\dot{m}$ until the relationship of figure 14 was satisfied at each time step. The solution was started by assuming a value of the entrance T_g, and $\dot{m}$ was computed from the orifice-flow relationship by using measured cove exit pressure and an initially assumed exit temperature. The exit gas temperature and $\dot{m}$ were determined iteratively so that the exit temperature agreed with the cove gas temperature at the exit defined by the present analysis. For each assumed entrance T_g, there were corresponding values of $\dot{m}$ and exit gas temperature that produced the measured pressure; and the corresponding value of T_s was then used with figure 14 to obtain a new entrance T_g to compare with that assumed. This iteration continued until the proper entrance T_g was established. Then this procedure just outlined was repeated for each time step to yield a transient solution of cove wall- and gas-temperature distributions.

Cold-Wall Heating Rates

Typical calculated cold-wall heating-rate distributions along the cove for various leak-slot areas are presented in figure 15 as solid-line curves and are compared with test data from reference 4. The ticked symbols represent the heating on the elevon side of the cove, and the unticked symbols represent heating on the wing side of the cove. (See fig. 11.) The calculated heating-rate distributions agree with the data for the first half of the cove where the cove gap height is constant. However, the prediction is generally low for the cove transition region (varying cove height) and at the cove seal near the cove exit, since the analysis did not include the factors that would naturally produce increased heating associated with varying cross-sectional area.

The cold-wall heating rates at three locations are correlated with mass flow in figure 16. The data include all of the leak slots tested that are listed in the table inset of figure 12. The correlation is best at the high flow rates where fewer experimental errors would be expected.

Gas Temperature

The experimentally determined cove gas temperatures obtained from exposed thermocouple beads in the investigation of reference 4 are presented in figure 17 for various leak areas at two cove locations, $x/L = 0.188$ and 0.688. The solid-line curves are the predicted gas temperature obtained from the present analysis. The dashed-line curves represent the predicted thermocouple temperature calculated by using a lumped-parameter model of the thermocouple and with the predicted gas temperature. (The lumped-parameter computer code is described in ref. 12.) The lumped-parameter model is illustrated in the inset of figure 17

and accounts for the mass of the thermocouple, the convection from the gas in the cove, and radiation losses from the thermocouple. For $x/L = 0.188$ (fig. 17(a)), the thermocouple data are well below the predicted values from the present analysis. The predicted thermocouple response shows better agreement with the thermocouple data, which indicates that there was a considerable effect of thermal mass on the gas-temperature measurements. Moreover, the gas-temperature gradient along the cove near the entrance is very high so that the predicted gas temperature is very sensitive to the accuracy of x/L. At $x/L = 0.688$ (fig. 17(b)), the thermocouple data approached the predicted gas temperature (solid-line curves), and the predicted thermocouple temperature (dashed-line curves) accounted for the initial temperature response of the thermocouple. Therefore, the gas temperatures predicted by the present analysis seem reasonable.

Wall Temperature

The experimentally determined wall temperatures from reference 4 for various leakage areas at two cove locations, $x/L = 0.06$ and 0.78, are presented in figure 18. Wall temperatures were obtained from thermocouples attached to thin disks surrounded by thicker walls which produced local lateral conduction due to the local temperature differences of the wall. The predicted temperature for a wall thickness equal to the thin disk, shown by the solid-line curves, agreed with experiment for the first few seconds, but the experimental results then fell below the predictions because of lateral conduction. The predicted thermocouple temperature, shown by the dashed-line curves, was computed by using a lumped-parameter analysis (ref. 12) of these discrete locations (see inset sketch of wall thermocouple model in fig. 18(b)) to account for the conduction effect. The convective heat load was the same as that which produced the solid-line curves from the basic cove analysis. This adjustment to the present analysis gives better agreement, but the basic analysis cannot accurately account for lateral conduction or variance in wall cross-sectional area.

The elevon-cove thermal analysis appears to be useful in a general analysis of the cove heating problem. The prediction of wind-tunnel results from short exposure times indicates that the gas temperature entering the cove can be determined from the external boundary-layer analysis. Also, the cold-wall heating rates and gas-temperature distributions of the cove can be reasonably predicted. The cove wall-temperature distributions are predictable if the wall structure can be represented as a plate with one-dimensional conduction. To predict more accurate structural temperatures, the techniques used herein to represent the convective heat load can be incorporated into a more detailed structural model which could more accurately represent the cove geometry and thermal-mass distribution.

THERMAL RESPONSE OF COVE TO SIMULATED TRAJECTORY

The results from experiments on cove response to test conditions that simulate a shuttle entry reported in reference 5 could be analyzed by the present analysis if the boundary-layer flow information for the test facility had been available. Unlike the procedure used for correlation of wind-tunnel test

results in the previous section, the procedure for predicting cove response to entry conditions includes a long-exposure condition where internal radiation would be a significant factor. Since the required boundary-layer flow information was not available, a comparison with reference 5 could not be made; consequently, the present analysis was instead applied to a shuttle-entry trajectory to demonstrate its computational capability to predict cove gas and wall temperatures. The results from this analysis are considered as a rough estimate of the cove thermal response because of the limited information available on local external-wing flow conditions and because of the inability of the present analysis to model the exact cove structure. Typical entry hot-wall heating-rate and pressure histories at the cove entrance from reference 5 are plotted in figure 19. The wing-surface temperature was computed directly from the heating-rate history (assuming radiation equilibrium with an emissivity of 0.8), and in this case the wing temperature was used as the entrance gas temperature. Obviously, a more accurate gas-temperature value could be obtained if knowledge of the approaching boundary layer were known and the methods outlined earlier in the analysis of the wind-tunnel results were used. The mass flow through the cove was computed by assuming a leakage gap area and the pressure drop across the cove seal for an orifice computation. The geometry, material properties, and gas properties were the same as the base-line values used in the parametric study.

In figure 20, typical computed gas- and wall-temperature variations with time at the cove exit during entry are presented for various cove-seal leak-area ratios. The dashed-line curve in figure 20(a) represents the wing-surface temperature used as the cove-entrance gas temperature. From these curves, it was determined that as A_l/A_c was increased from 0.03 to 0.50, the maximum exit temperatures increased from 66 to 89 percent of the maximum entrance gas temperature. These results indicate that hot-gas leakage for even the smallest leak areas considered herein would produce a greater temperature at the cove exit than the current shuttle designs could withstand. However, proper account is not made for the actual thermal mass of the shuttle-cove interior structure.

In considering the effect of structural mass using this analysis, additional computations were made of the thermal effects on the shuttle cove-seal rub tube located at the cove exit. A lumped-parameter computation was made by assuming that the entire rub tube (illustrated by the inset in fig. 21) was at a uniform temperature resulting from a convective heat load over half of the surface area and from radiation away from the other half. The computed rub-tube temperature histories for various leakage areas and two initial temperatures are presented in figure 21. The results in figure 21(a) correspond to the exit temperatures of figure 20 for a "hot-start" where T_i = 295 K. The results in figure 21(b) represent a "cold-start" condition where the shuttle is cooled to T_i = 185 K while in orbit. For each plot the dashed line represents the design rub-tube temperature limit of 450 K. Obviously, greater leak areas can be tolerated for the lower initial structural temperature (fig. 21(b)). The maximum rub-tube temperatures for these two initial conditions are plotted as a function of leak gap in figure 22. The allowable leak gap indicated for the "hot-start" condition is about 0.044 cm which is within about 20 percent of the experimentally determined value of reference 5.

The possible benefit of varying the cove internal radiation by means of cove gap height or surface emissivity, as suggested in the parametric study, was considered in the present application to entry conditions. For example, the cove exit wall-temperature histories for $A_l/A_c = 0.06$ are presented for $\varepsilon = 0.8$ and 0 in figure 23. Initially, the cove interior temperature was reduced by a reduction in radiation, but eventually this trend was reversed similar to that shown earlier by the parametric study in figure 7. In figure 23 the maximum exit wall temperature, which occurred in the later portion of the entry, increased substantially as the internal radiation was reduced. The reduction of cove internal radiation would probably be beneficial for very small leakage areas (low mass-flow rates), lower than those included in this study.

CONCLUDING REMARKS

A mathematical model of the heating associated with leakage within a shuttle-type wing-elevon cove was used to analyze the aerothermal response of the structure. Flow in the cove was modeled as developing channel flow between parallel plates. The mass flow entering the cove was assumed to be the portion of the external-flow boundary layer that is next to the wing surface ahead of the cove. A parametric study described the mechanism by which the energy of the ingested mass is distributed as a function of the Reynolds number, wall conductivity, surface emissivity, and cove height and length. The results indicated that the rate at which energy was transferred into the cove interior was primarily determined by the relationship of the convection, wall capacitance, and internal radiation. Initially, low internal radiation reduced energy penetration into the cove; but when the interior temperature increased sufficiently, radiation helped cool the interior.

Correlation of wind-tunnel results from another investigation indicated that the cold-wall heating rates, wall temperature, and gas temperature of the cove were predictable by using the present analytical model. Thus, assumptions used herein were correct. Predicted thermal response of the elevon cove subjected to shuttle-entry conditions indicated that the allowable leak area at the cove seal was 20 percent less than that previously indicated by experimental results. To predict more accurate structural temperatures, the techniques used herein to represent the convective heat transfer must be incorporated into a more detailed structural model which would more accurately represent the cove geometry and thermal mass distribution.

Langley Research Center
National Aeronautics and Space Administration
Hampton, VA 23365
August 11, 1980

REFERENCES

1. Strouhal, George; and Tillian, Donald J.: Testing the Shuttle Heat-Protection Armor. Astronaut. & Aeronaut., vol. 14, no. 1, Jan. 1976, pp. 57-65.

2. Dearing, J. David; and Hamilton, H. Harris: Heat-Transfer and Pressure Distributions Inside the Hinge-Line Gap of a Wedge-Flap Combination at Mach Number 10.4. NASA TN D-4911, 1968.

3. Stern, I.; and Rowe, W. H., Jr.: Effect of Gap Size on Pressure and Heating Over the Flap of a Blunt Delta Wing in Hypersonic Flow. J. Spacecr. & Rockets, vol. 4, no. 1, Jan. 1967, pp. 109-114.

4. Deveikis, William D.; and Bartlett, Whitney: Pressure and Heat-Transfer Distributions in a Simulated Wing-Elevon Cove With Variable Leakage at a Free-Stream Mach Number of 6.9. NASA TM-74095, 1978.

5. Scott, C. D.; Murray, L. P.; and Milhoan, J. D.: Shuttle Elevon Cove Aerodynamic Heating by Internal Flow. AIAA Paper 77-757, June 1977.

6. Cooper, Larry; and Putz, Kurt E.: Generalized Flow in Gaps and Slots Including the Effects of Ablation. J. Spacecr. & Rockets, vol. 11, no. 5, May 1974, pp. 287-294.

7. Keshock, Edward G.: Analysis of Heat Transfer in a Simulated Wing-Elevon Cove in Hypersonic Flow. AIAA Paper 78-40, Jan. 1978.

8. Kays, W. M.: Numerical Solutions for Laminar-Flow Heat Transfer in Circular Tubes. Trans. ASME, vol. 77, no. 8, Nov. 1955, pp. 1265-1274.

9. Kays, W. M.: Convective Heat and Mass Transfer. McGraw-Hill Book Co., Inc., c.1966.

10. Gebhart, Benjamin: Heat Transfer. McGraw-Hill Book Co., Inc., c.1961.

11. Howell, John R.; and Siegel, Robert: Thermal Radiation Heat Transfer. Volume II: Radiation Exchange Between Surfaces and in Enclosures. NASA SP-164, 1969.

12. Martin Interactive Thermal Analyzer System - Version 1.0. User's Manual. MDS-SPLPD-71-FD238 (Rev 3), Martin Marietta Corp., Mar. 1972.

13. Bartlett, Eugene P.; and Kendall, Robert M.: An Analysis of the Coupled Chemically Reacting Boundary Layer and Charring Ablator. Pt. III - Nonsimilar Solution of the Multicomponent Laminar Boundary Layer by an Integral Matrix Method. NASA CR-1062, 1968.

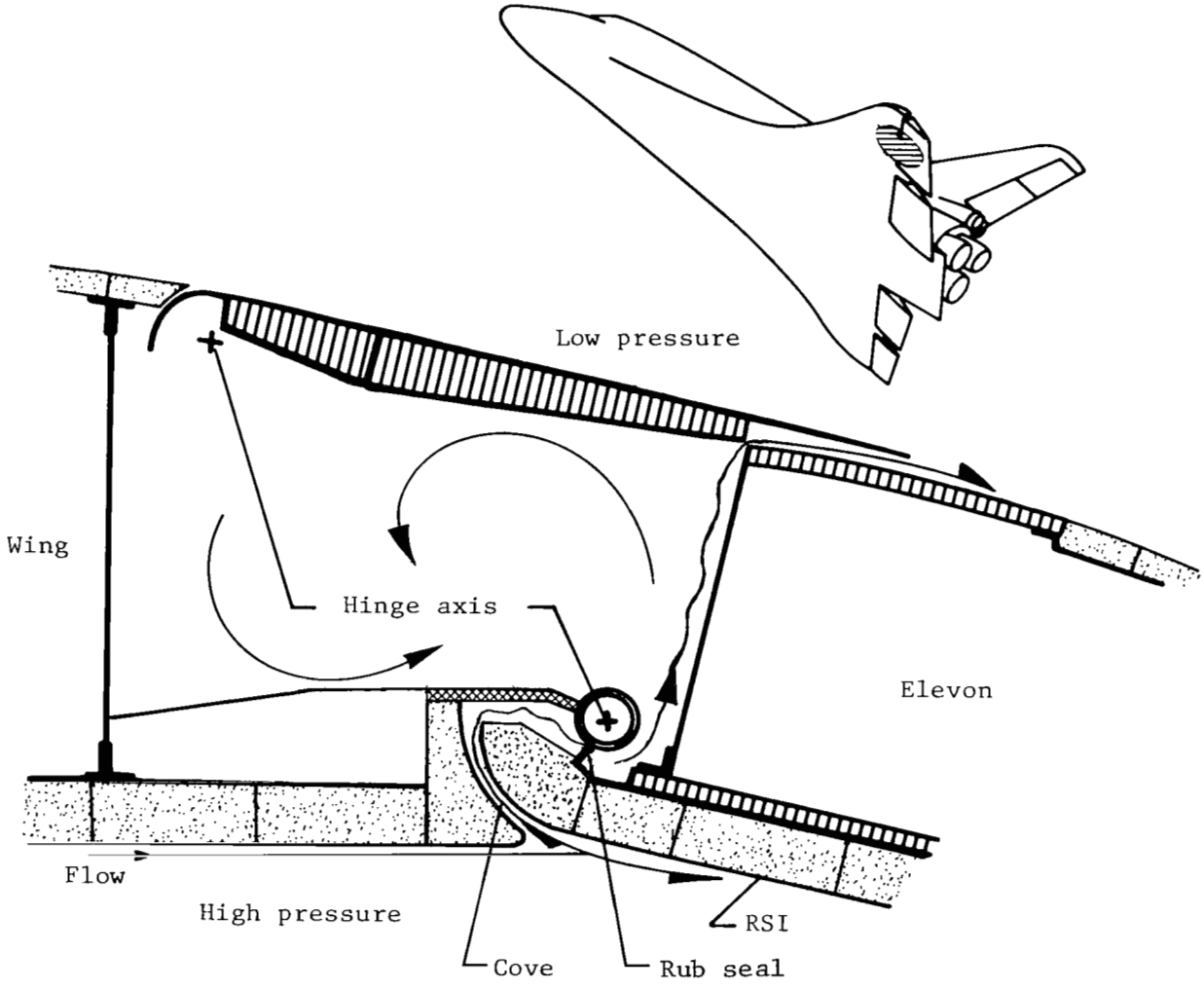

Figure 1.- Cross section of Space Shuttle Orbiter structure at wing-elevon juncture.

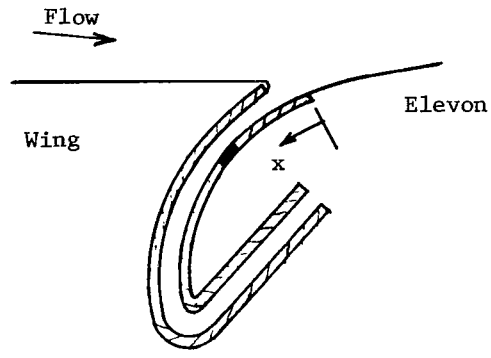

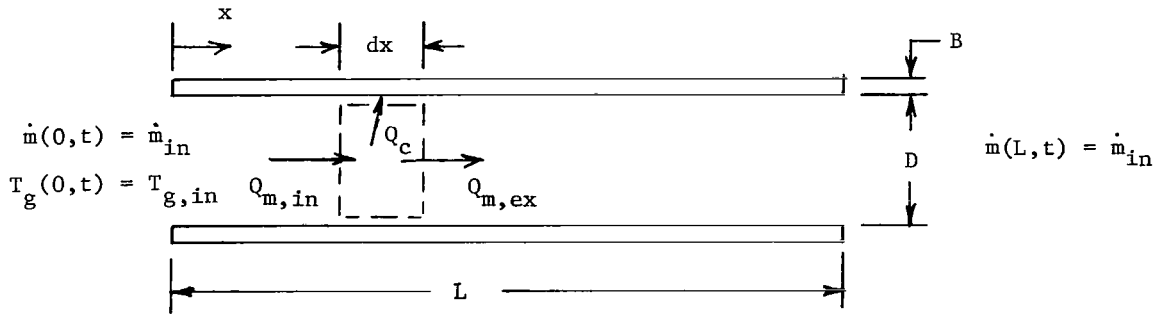

(a) Fluid model.

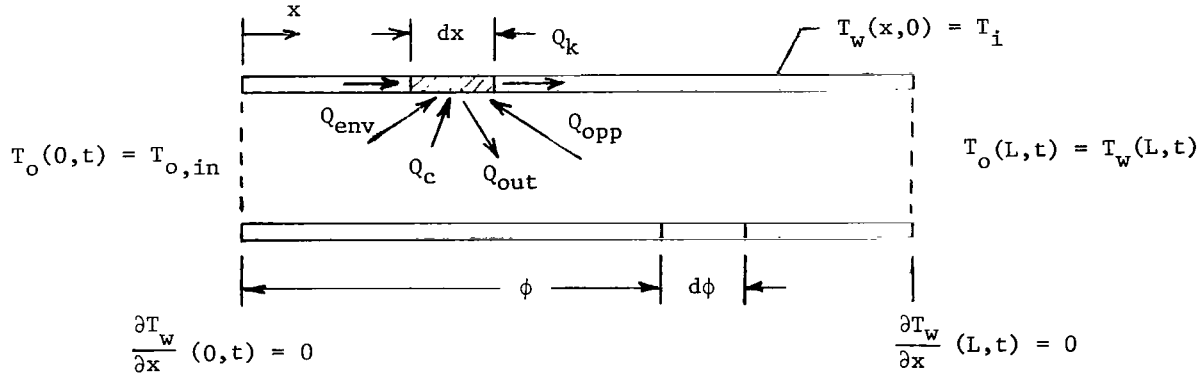

(b) Wall model.

Figure 2.- Illustration of math model of gas flow in cove.

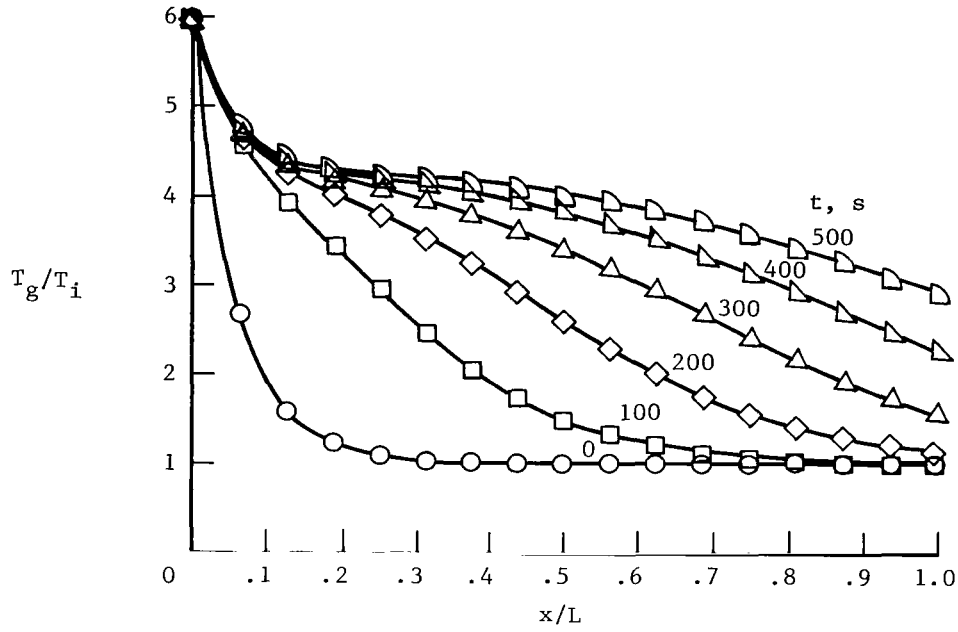

(a) Gas.

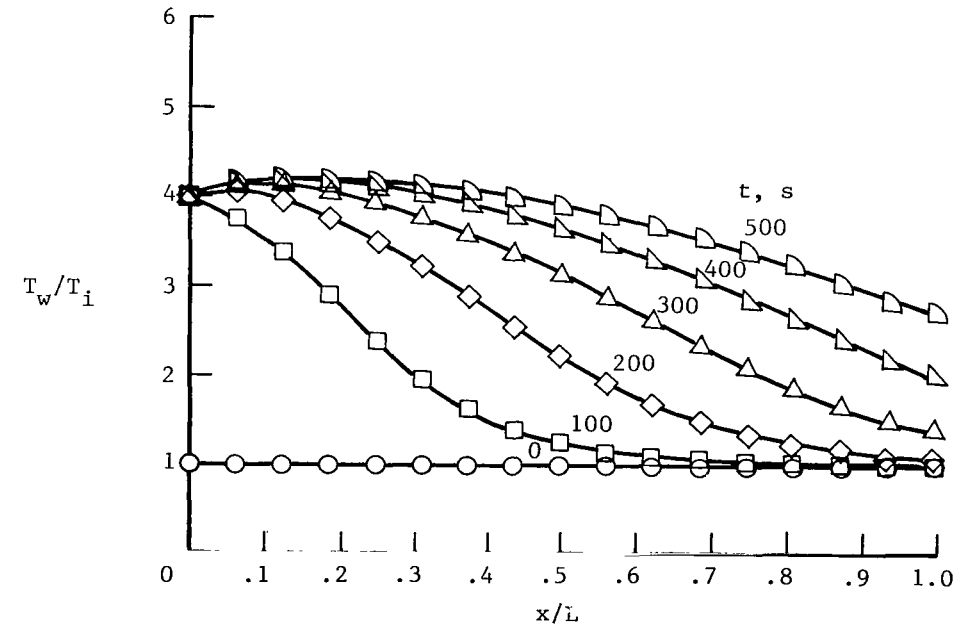

(b) Wall.

Figure 3.- Typical cove temperature distributions. $R_c = 50$; $T_{g,in}/T_i = 6$; $D = 1.27$ cm; $B = 0.64$.

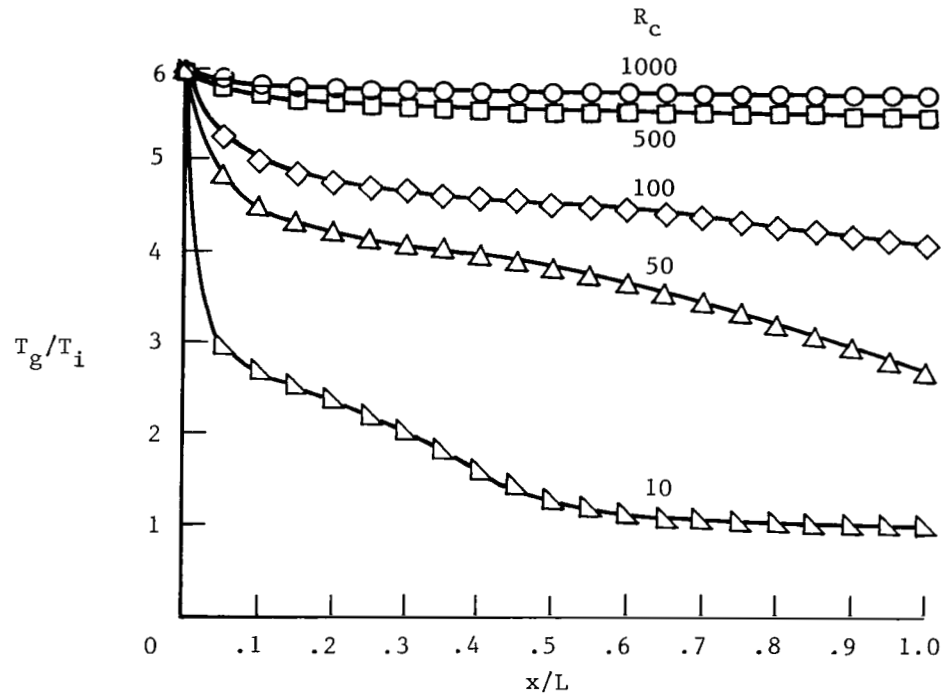

(a) Gas.

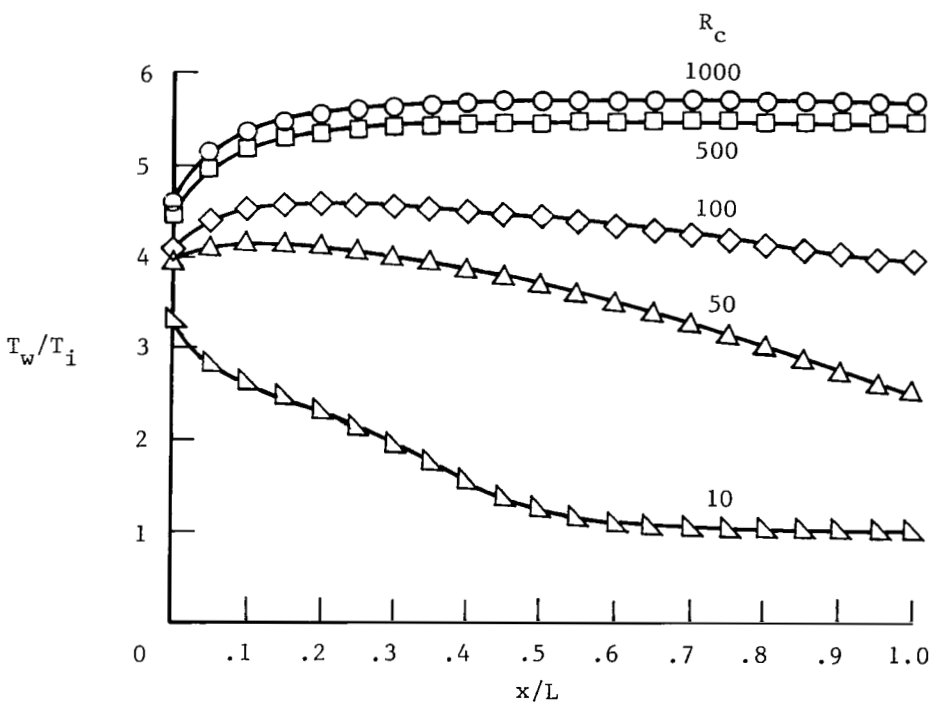

(b) Wall.

Figure 4.- Variation of cove temperature with Reynolds number. $T_{g,in}/T_i = 6$; D = 1.27 cm; B = 0.64 cm; t = 500 s.

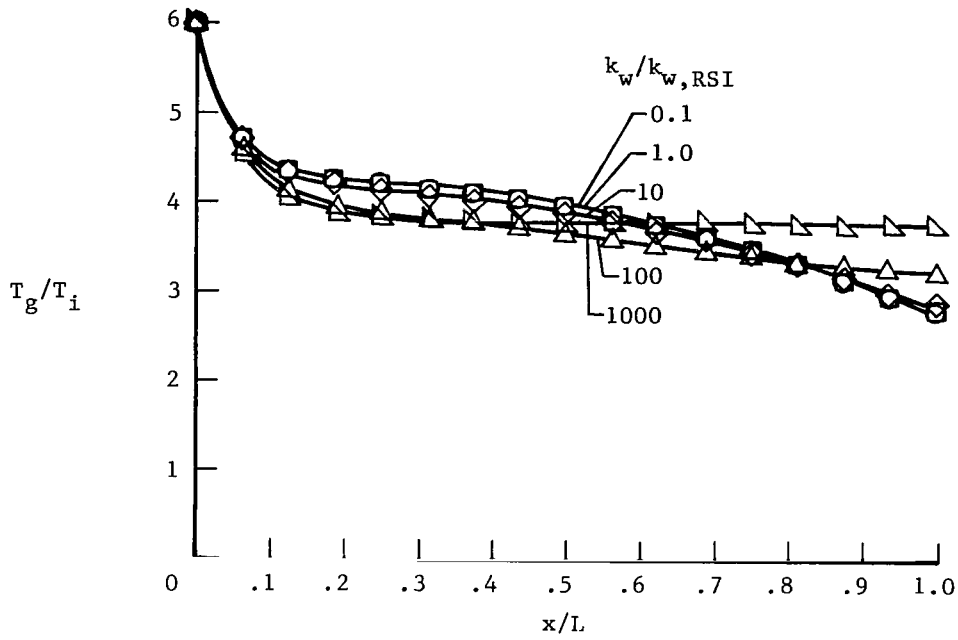

(a) Gas.

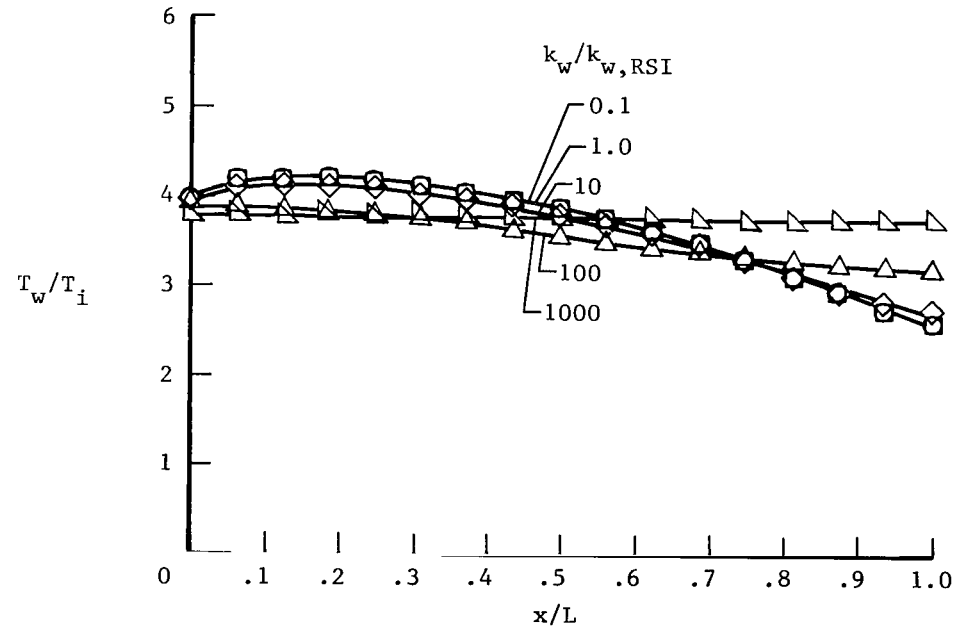

(b) Wall.

Figure 5.- Variation of cove temperature distribution with wall thermal conductivity. $R_c = 50$; $T_{g,in}/T_i = 6$; D = 1.27 cm; B = 0.64 cm; t = 500 s.

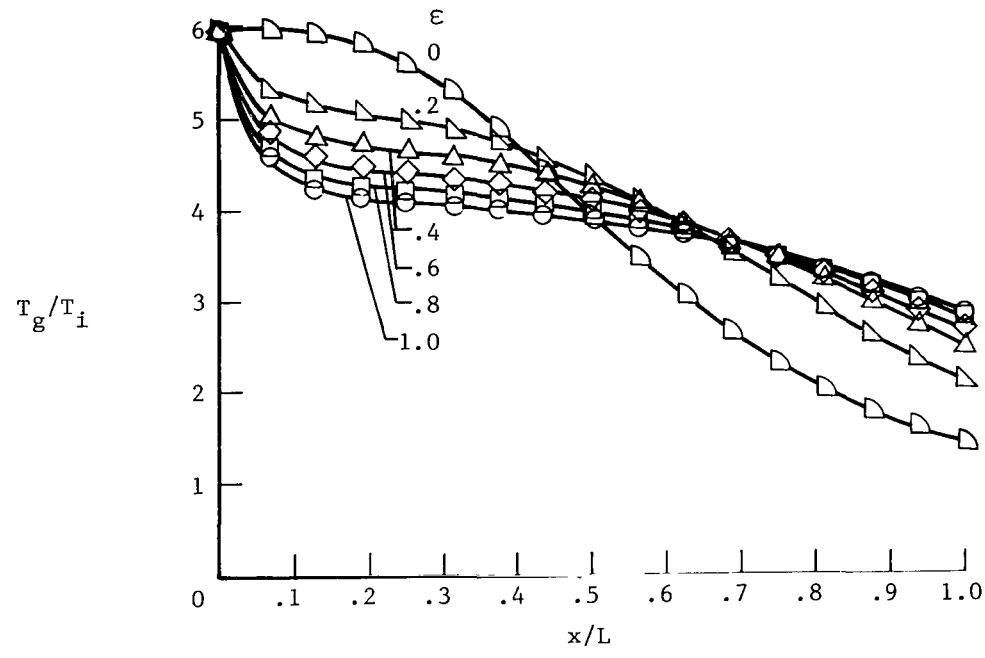

(a) Gas.

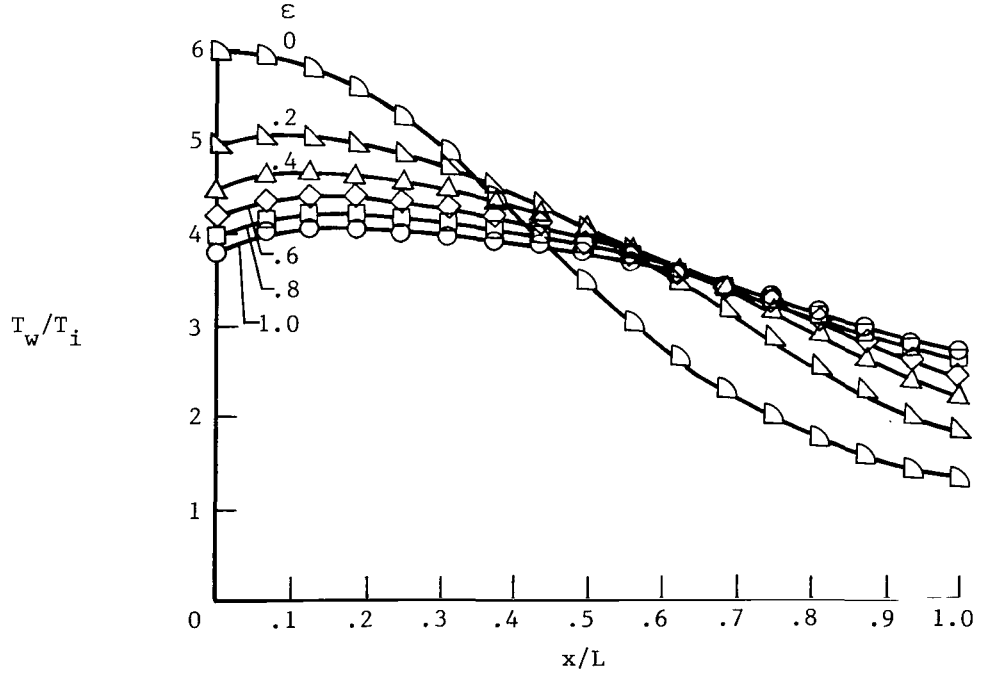

(b) Wall.

Figure 6.- Variation of cove temperature distribution with surface emissivity. $R_c = 50$; $T_{g,in}/T_i = 6$; D = 1.27 cm; B = 0.64 cm; t = 500 s.

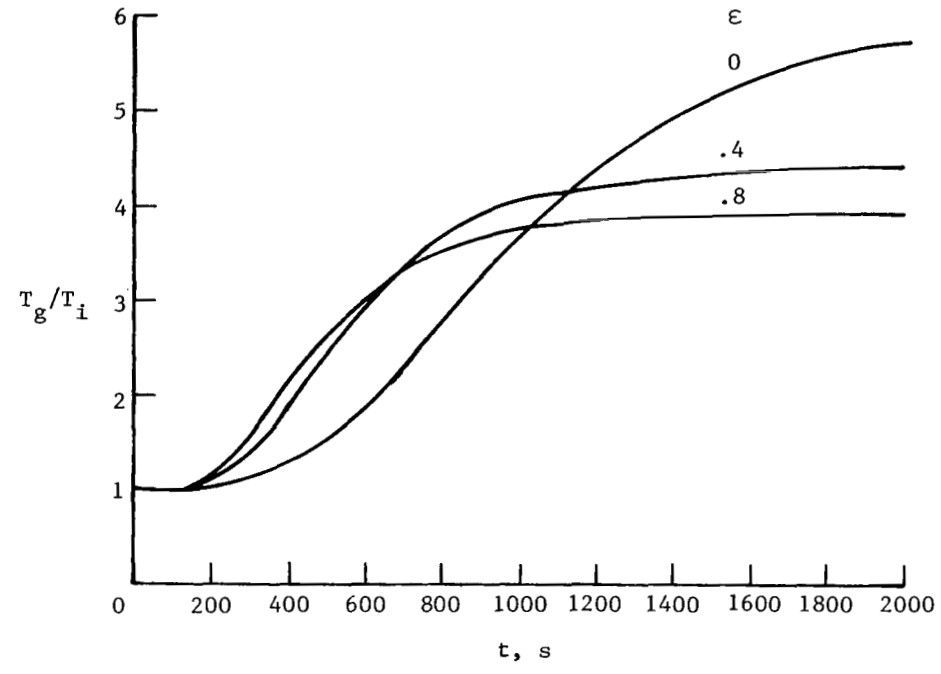

(a) Gas.

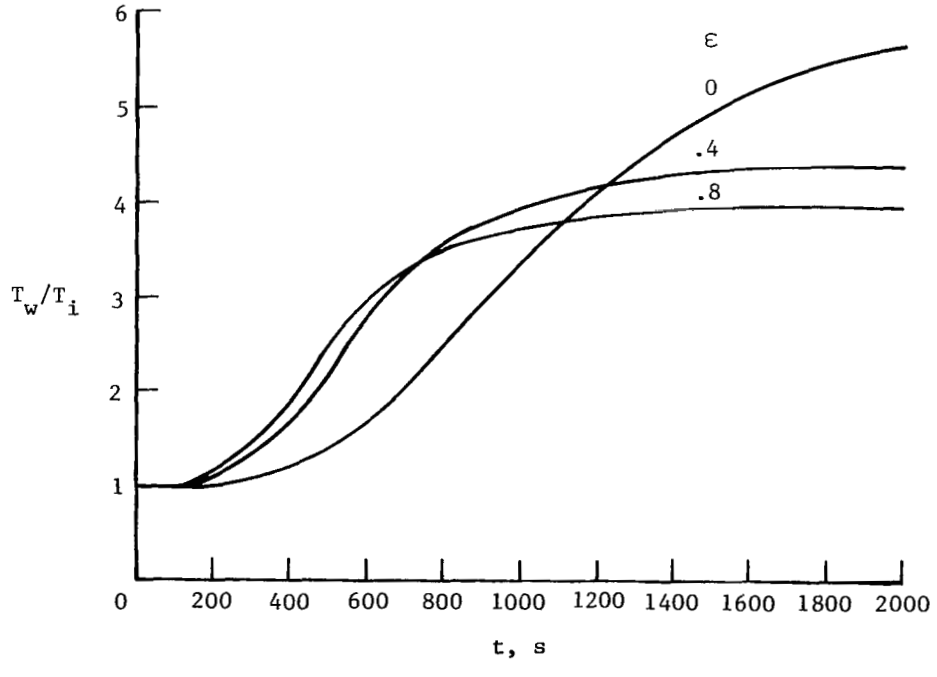

(b) Wall.

Figure 7.- Cove-exit temperature histories for various surface emissivities. R_C = 50; $T_{g,in}/T_i$ = 6; D = 1.27 cm; B = 0.64 cm.

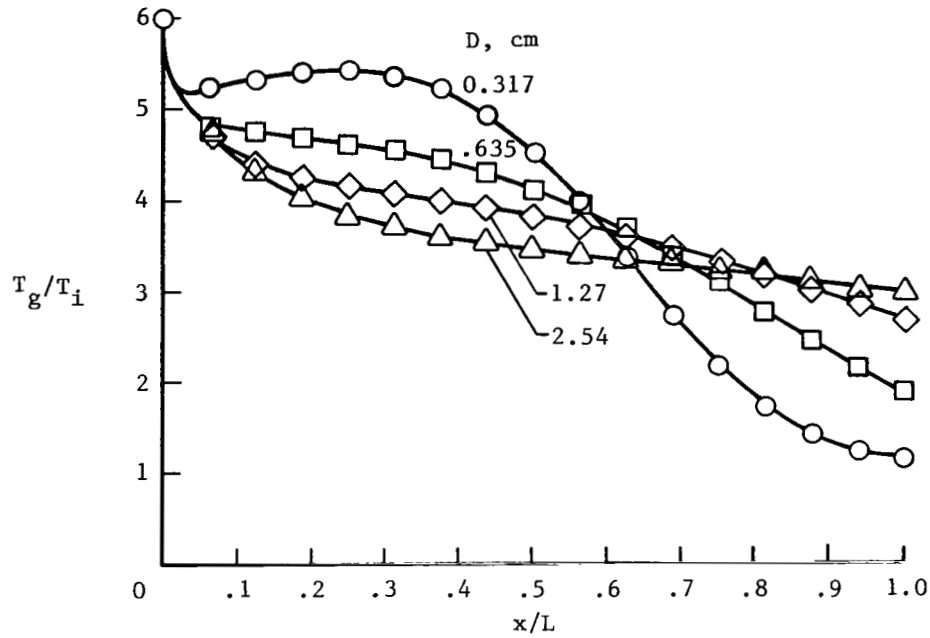

(a) Gas.

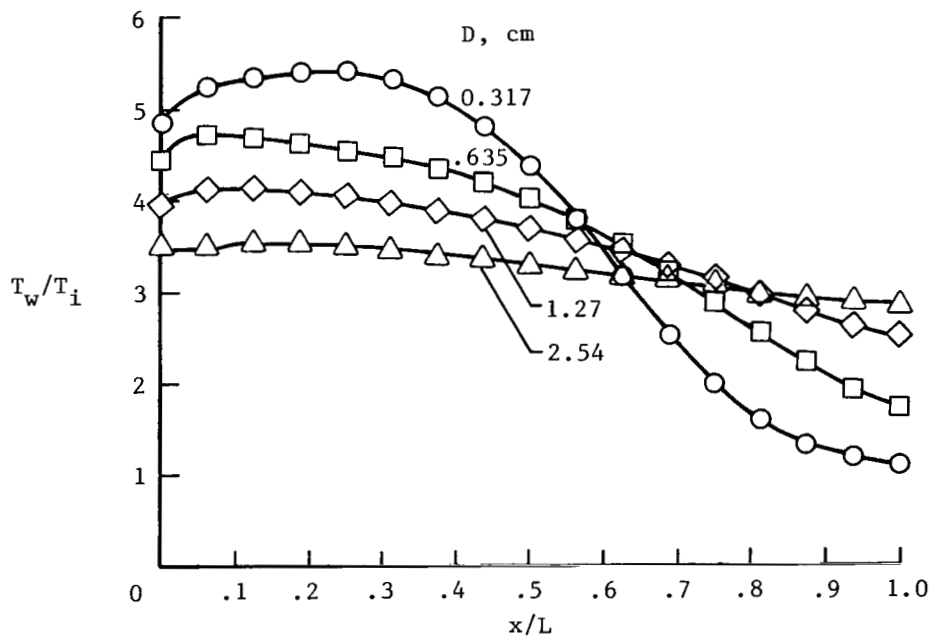

(b) Wall.

Figure 8.- Variation of cove temperature distribution with cove height. $R_c = 50$; $T_{g,in}/T_i = 6$; B = 0.64 cm; t = 500 s.

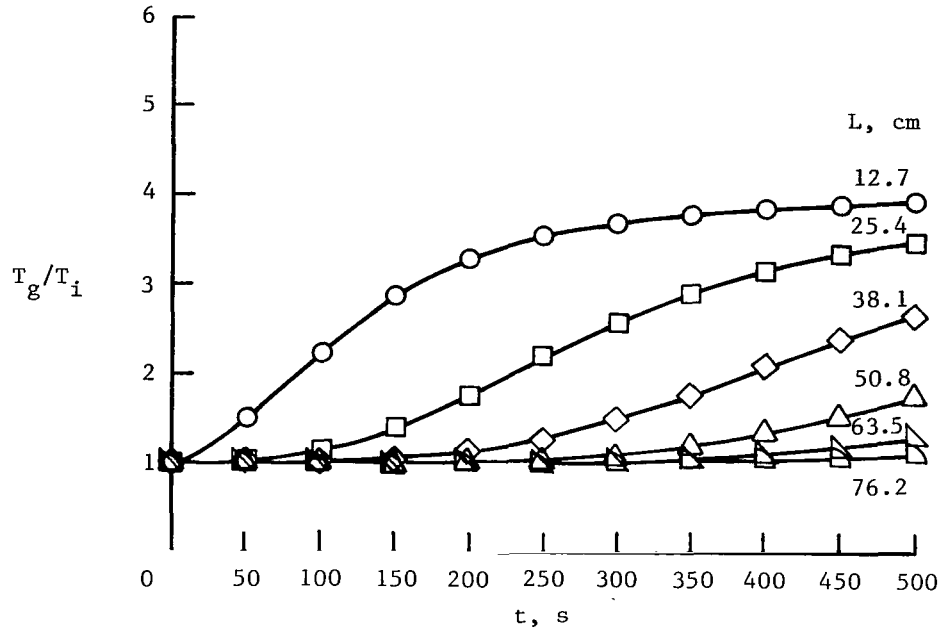

(a) Gas.

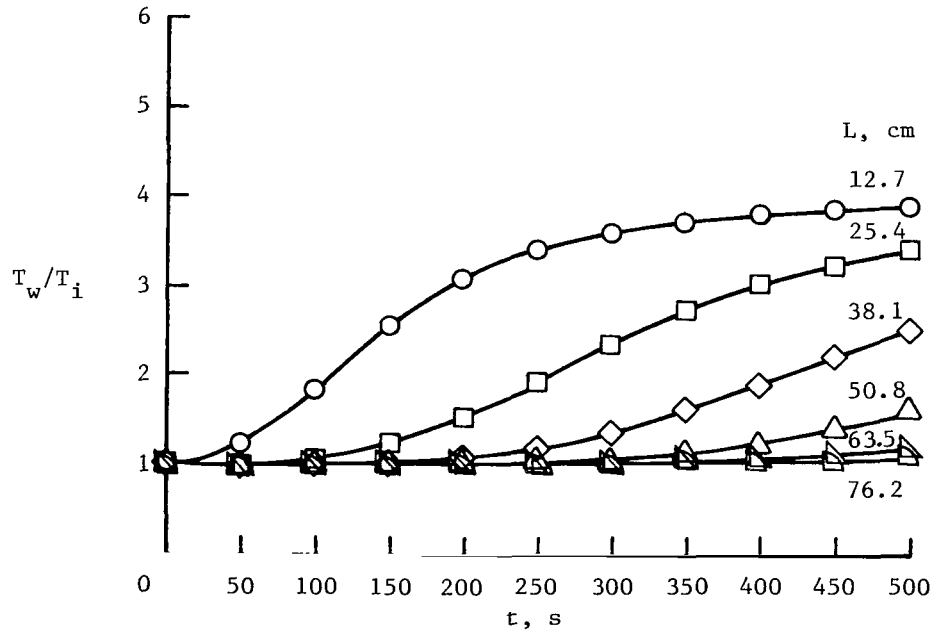

(b) Wall.

Figure 9.- Effect of cove length on cove-exit temperature history. $R_c = 50$; $T_{g,in}/T_i = 6$; D = 1.27 cm; x/L = 1; B = 0.64 cm.

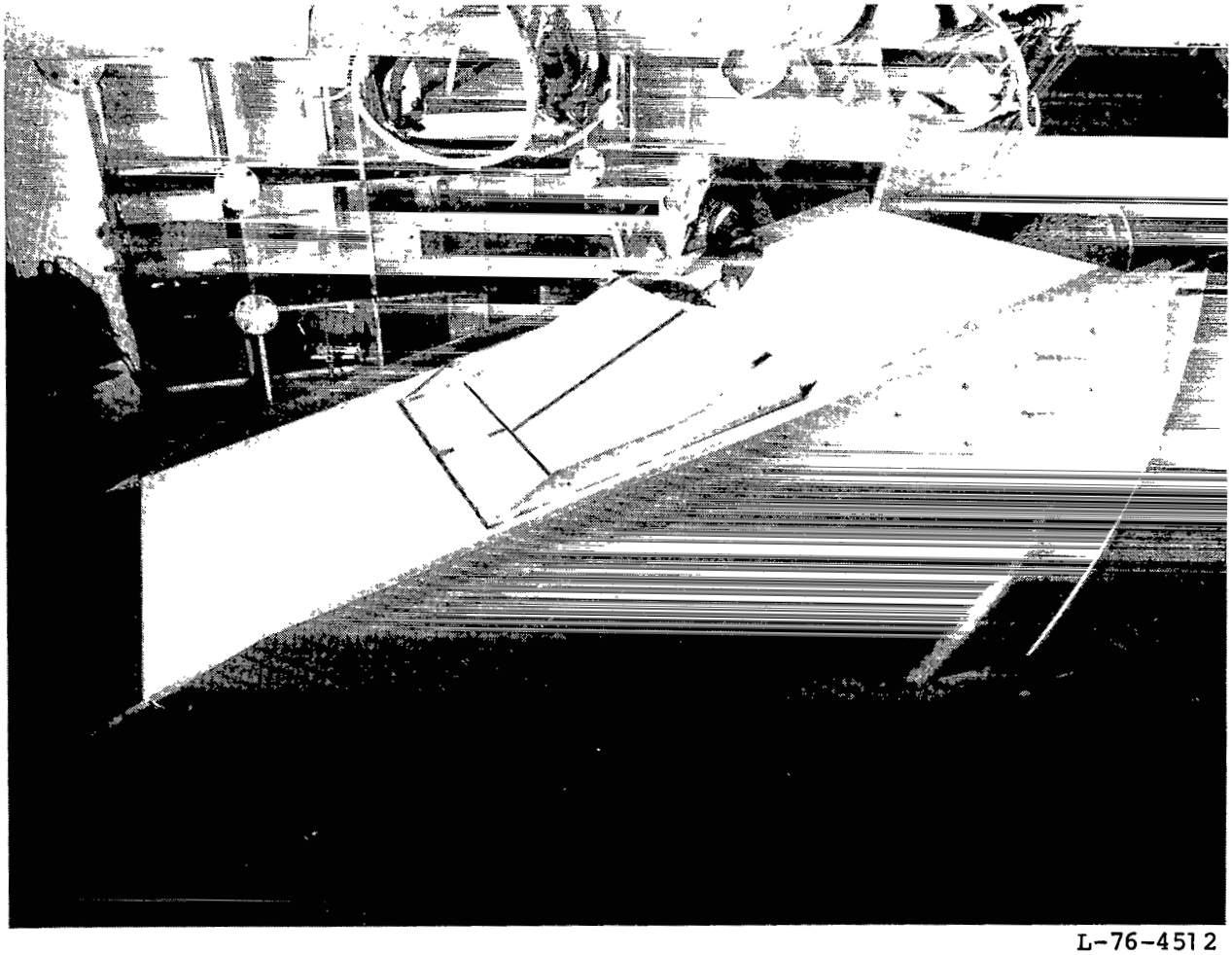

L-76-4512

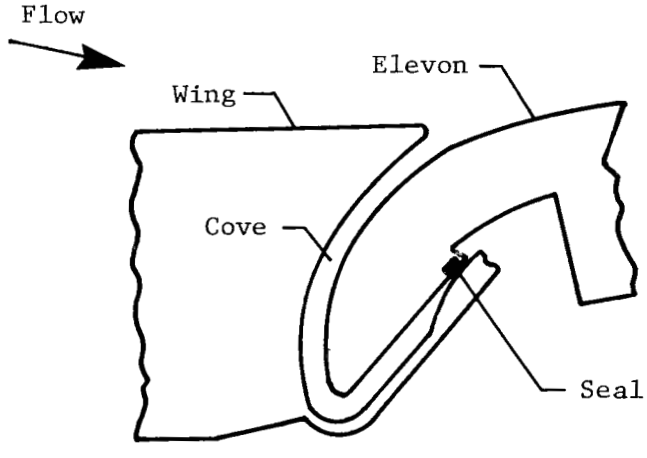

Schematic diagram of cove region

Figure 10.- Wing-elevon cove test apparatus (ref. 4).

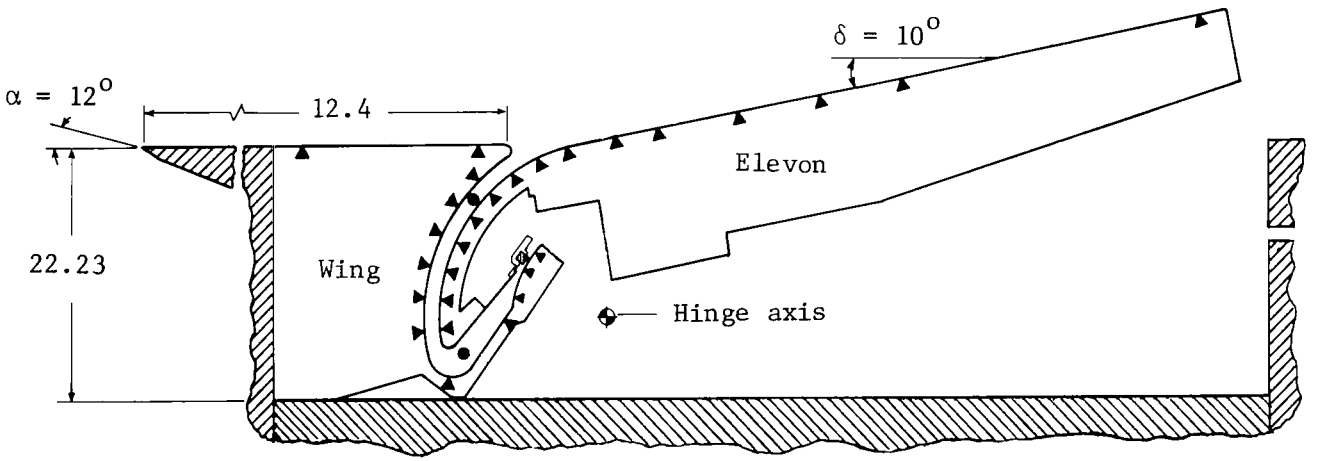

Symbol	Thermocouples
•	Cove gas thermocouple
▲	Wall thermocouple

Figure 11.- Cross section of model installed in test bed and center-line insrumentation distribution. Dimensions are given in centimeters.

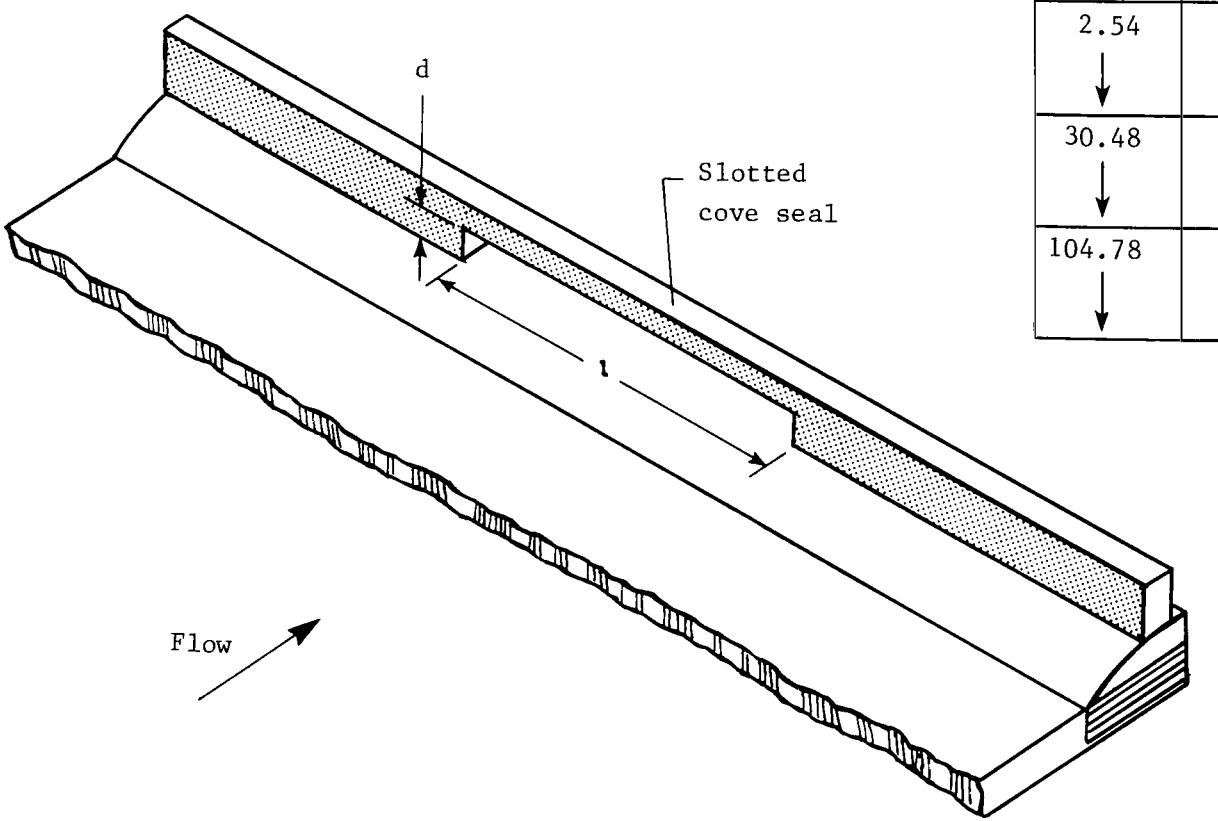

l, cm	d, cm	A_l/A_c
2.54	0.318	0.006
↓	.635	.012
	1.270	.024
30.48	0.318	0.073
↓	.635	.150
	1.270	.290
104.78	0.198	0.160
↓	.356	.280
	.686	.540

Figure 12.- Arrangement of cove seal and rub surface. Dimensions are given in centimeters.

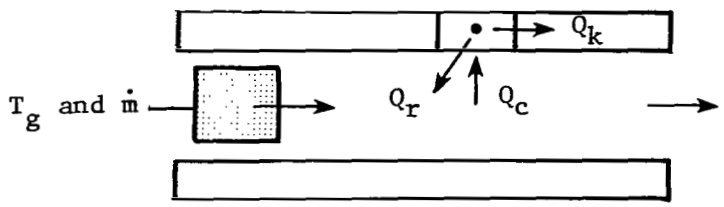

(a) Illustration of simplified math model.

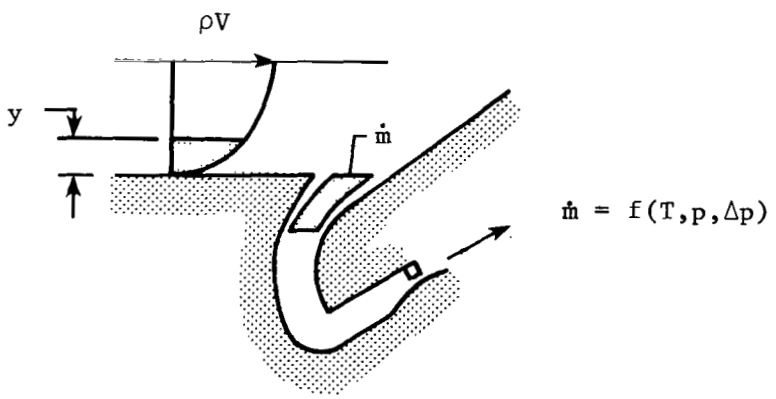

(b) Ingested mass-flow rate.

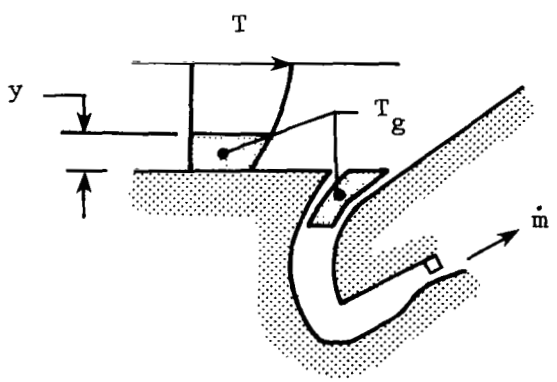

(c) Ingested mass temperature.

Figure 13.- External boundary-layer analysis to determine entrance gas temperature.

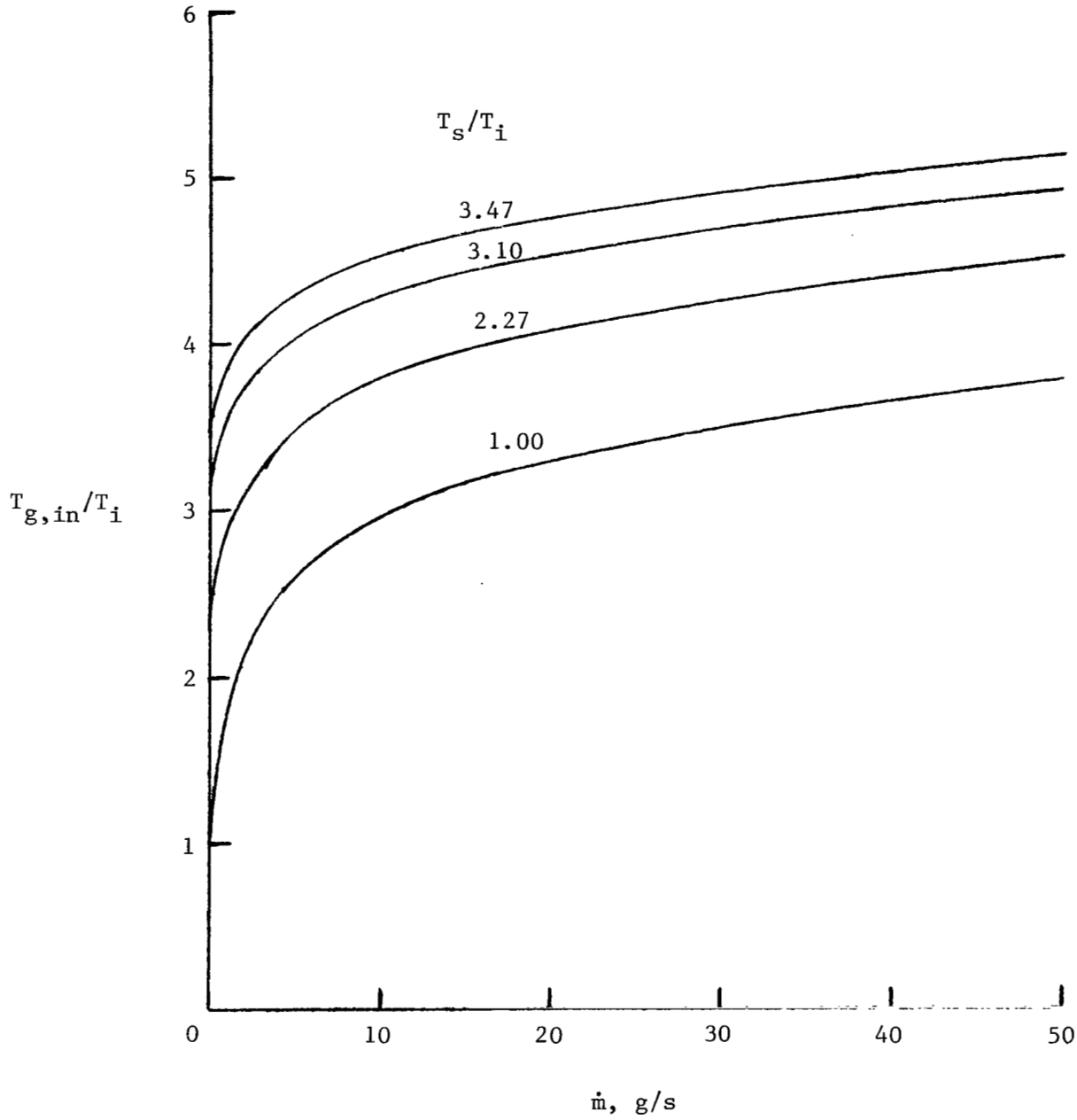

Figure 14.- Entrance gas temperature for variation of mass flow.
$R \approx 4.3 \times 10^6\ m^{-1}$; $T_i = 295$ K.

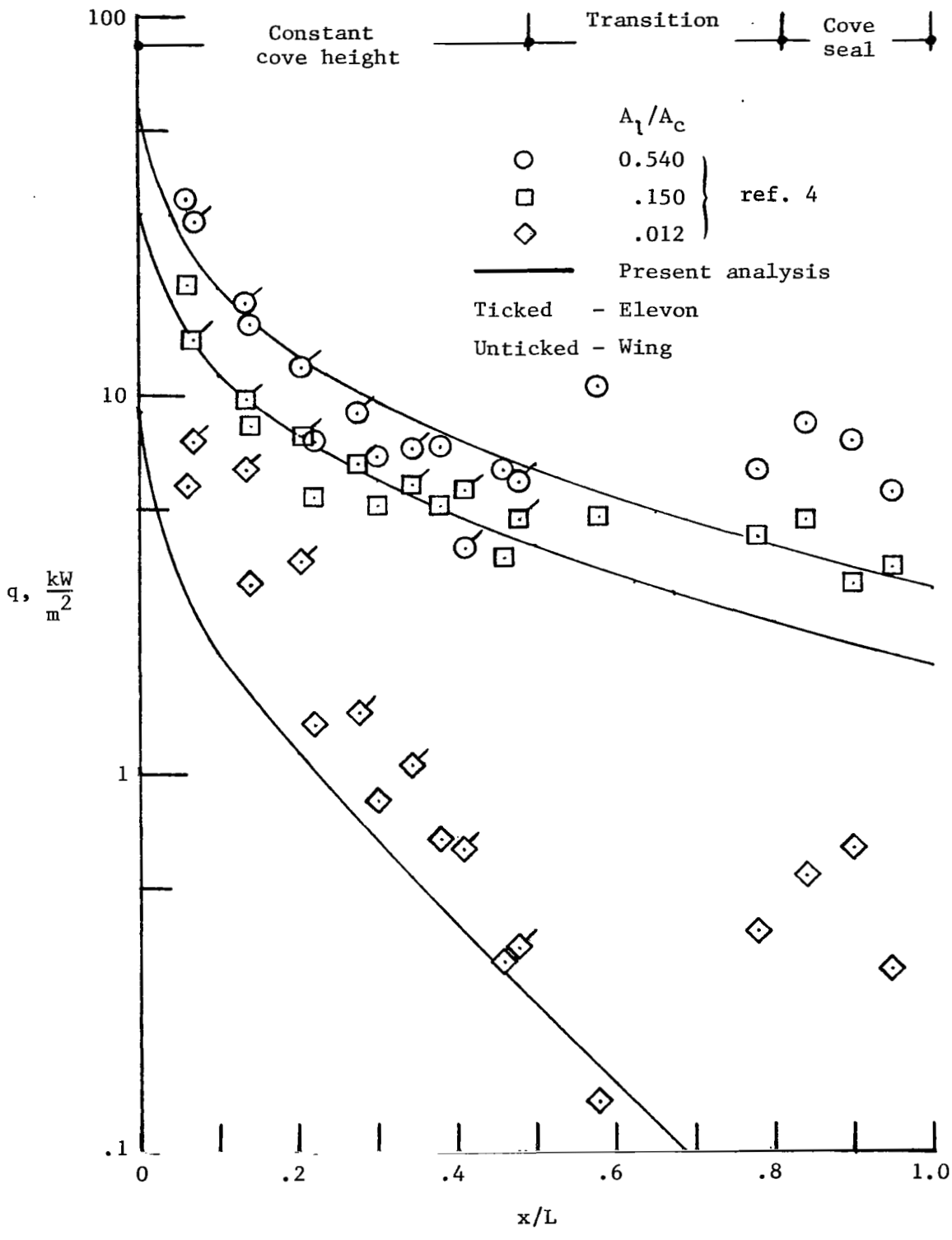

Figure 15.- Cold-wall heating-rate distributions along cove walls for various leakage areas.

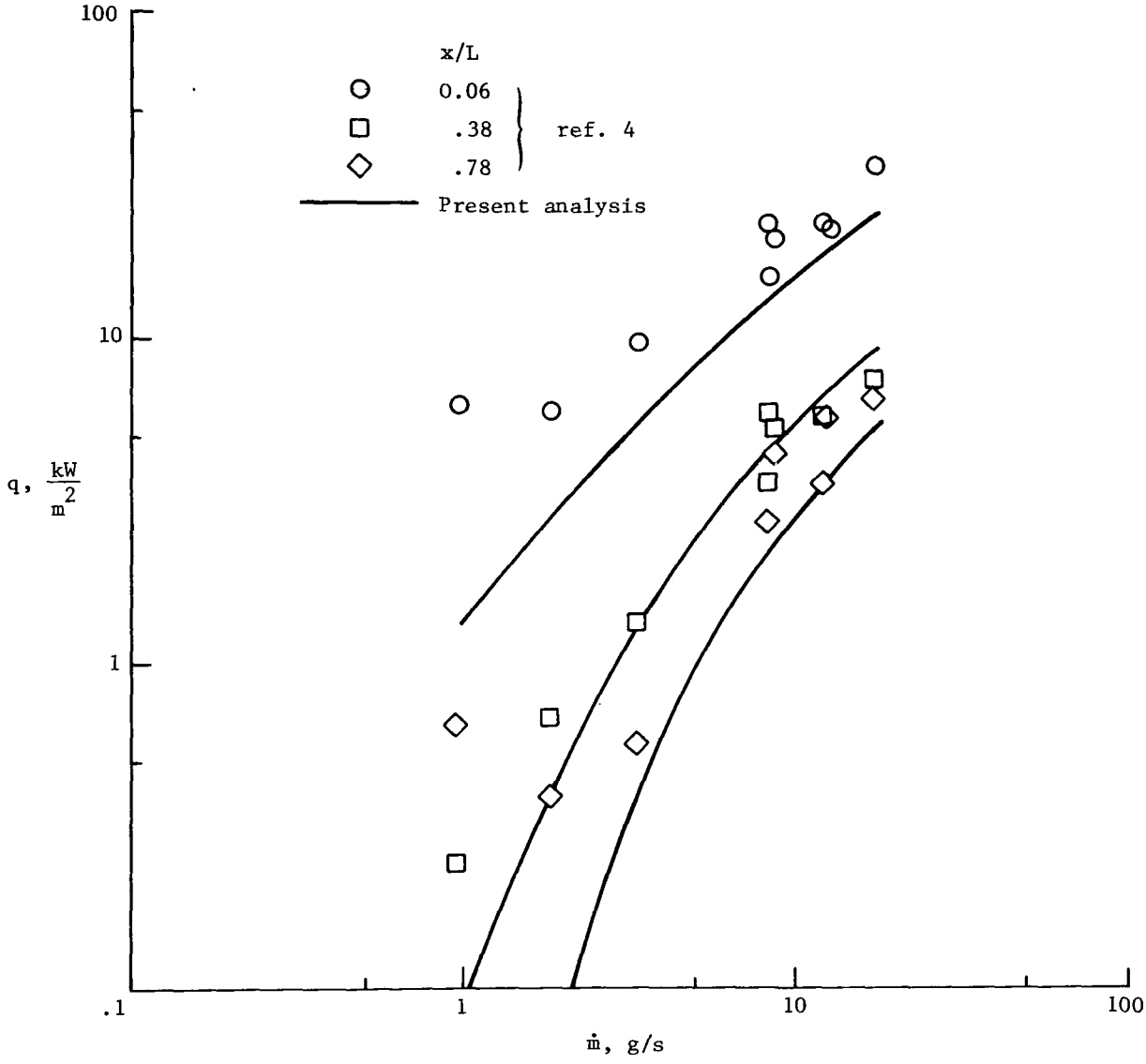

Figure 16.- Correlation of cold-wall heating rates with mass flow.

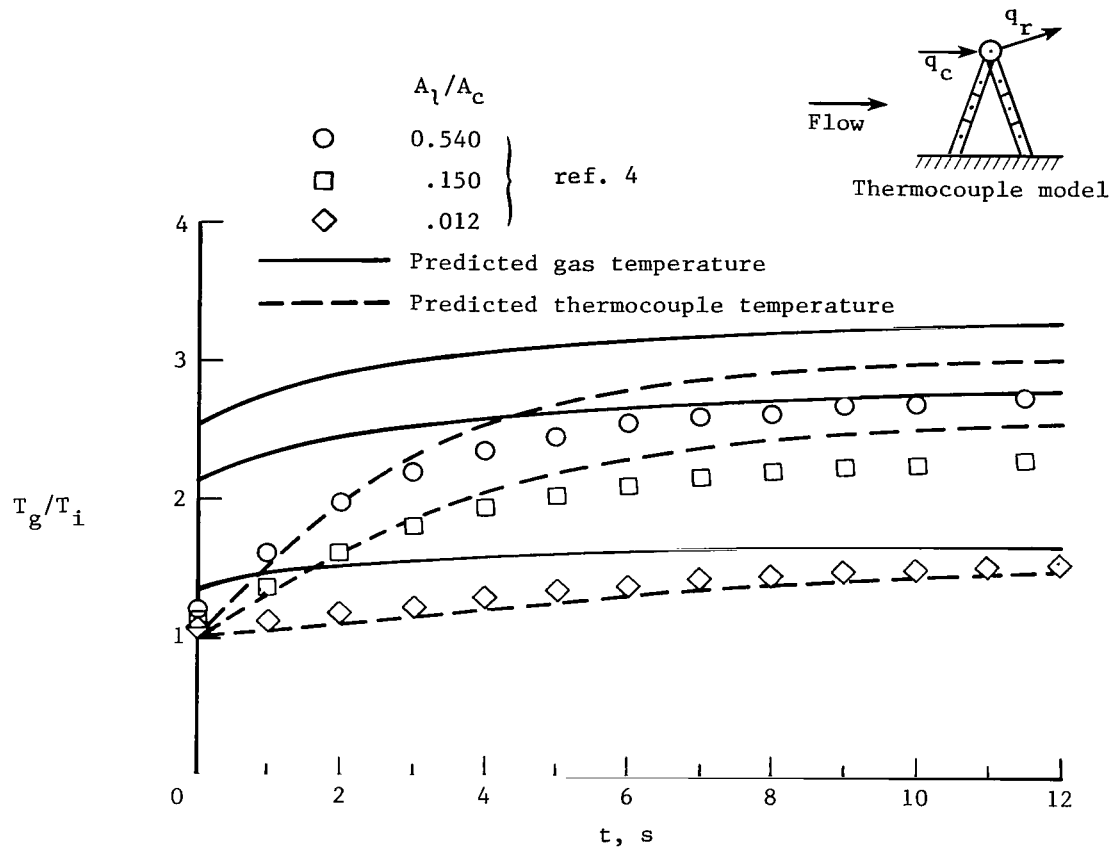

(a) x/L = 0.188.

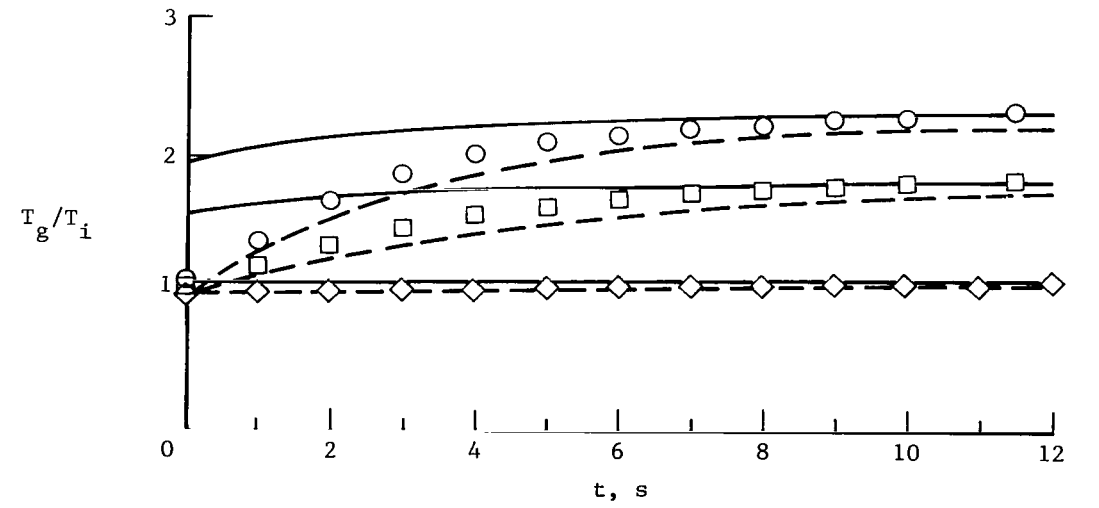

(b) x/L = 0.688.

Figure 17.- Gas-temperature histories for various leakage areas.

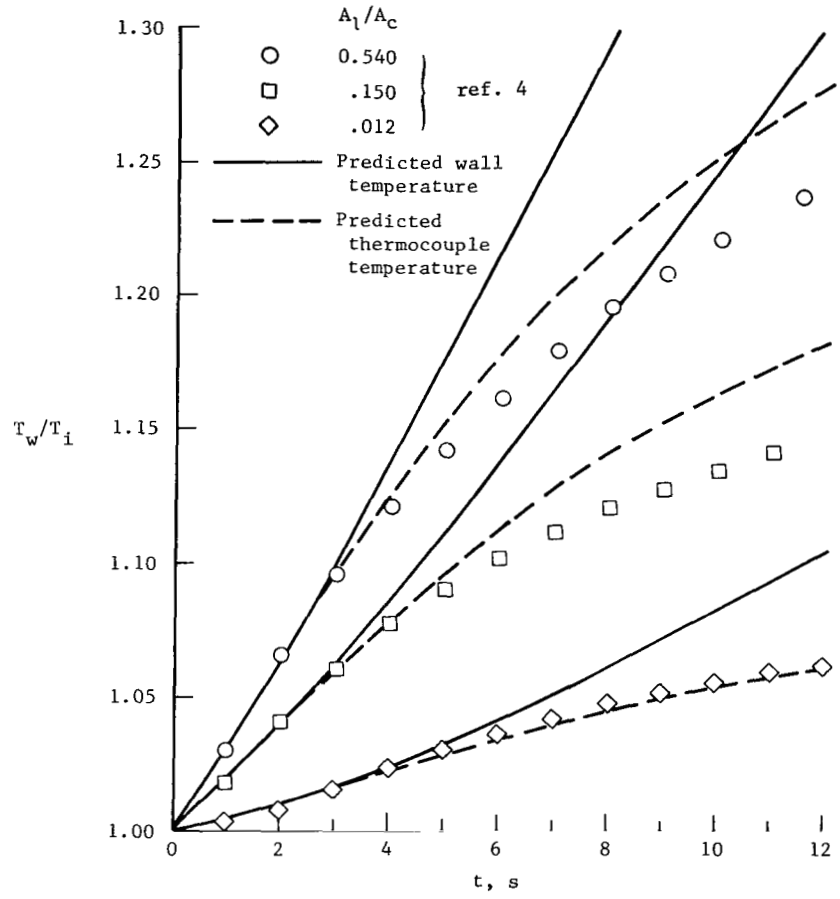

(a) x/L = 0.06.

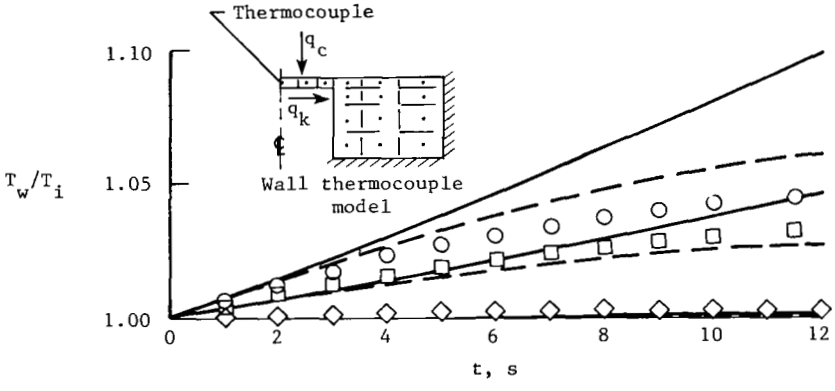

(b) x/L = 0.78.

Figure 18.- Wall-temperature histories for various leakage areas.

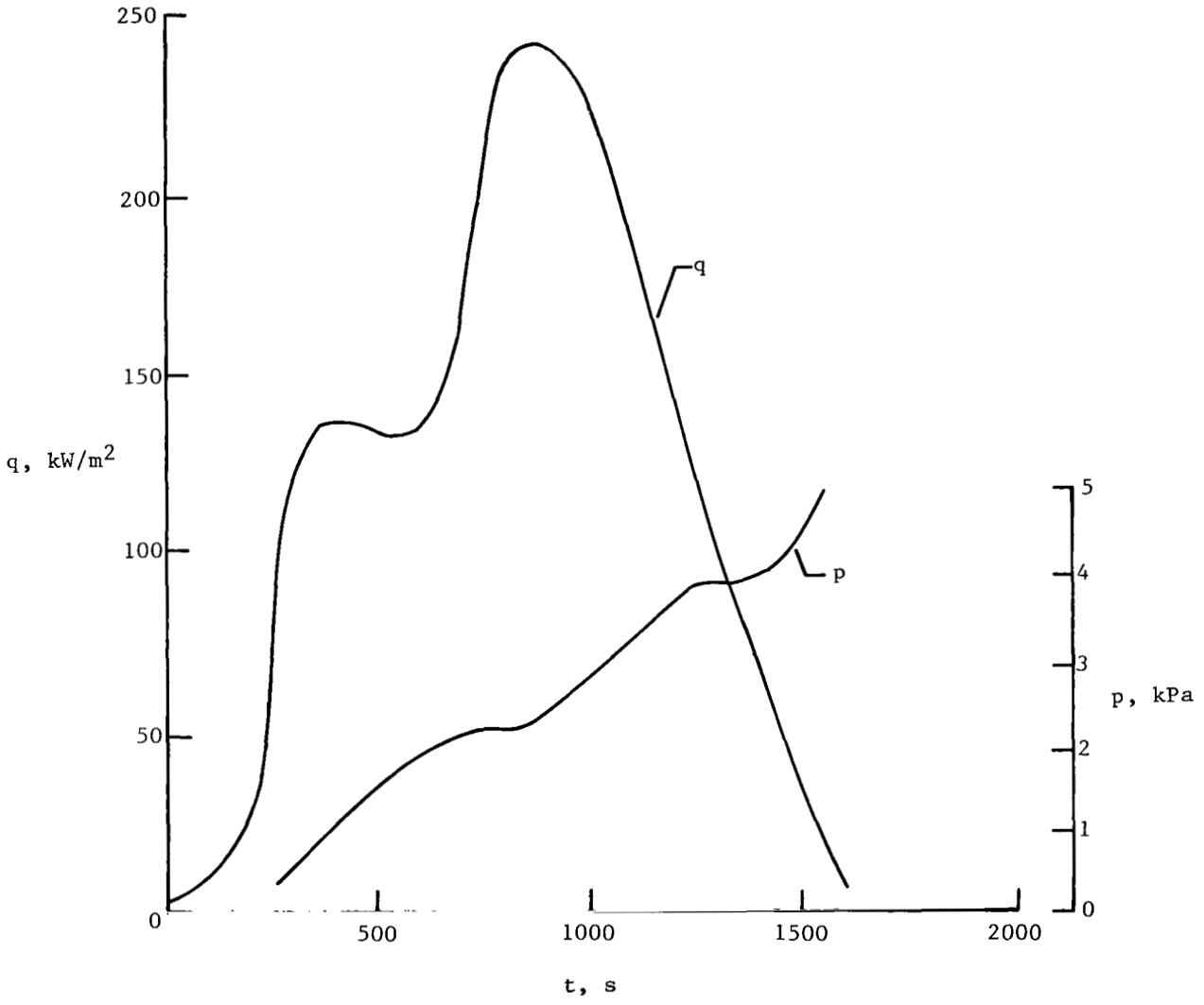

Figure 19.- Local environment for elevon cove during shuttle entry.

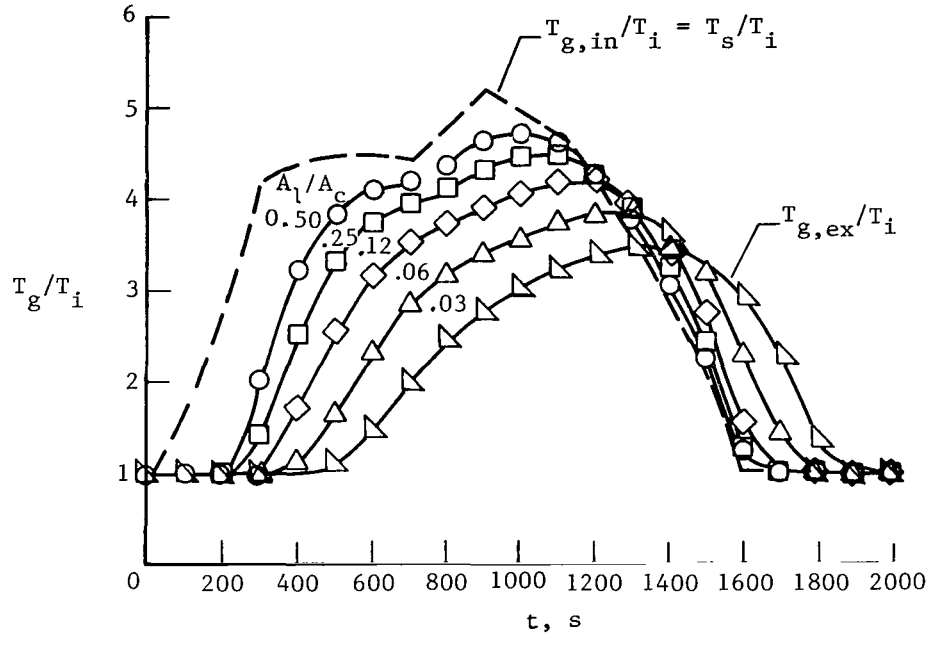

(a) Gas.

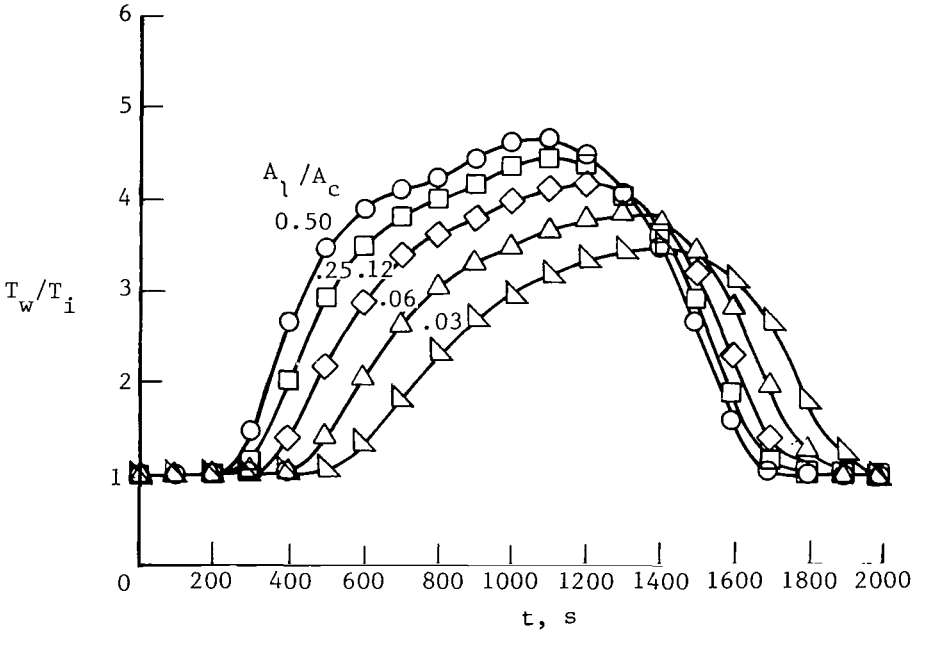

(b) Wall.

Figure 20.- Typical cove-exit temperature histories for various leakage areas exposed to shuttle trajectory. T_i = 294 K.

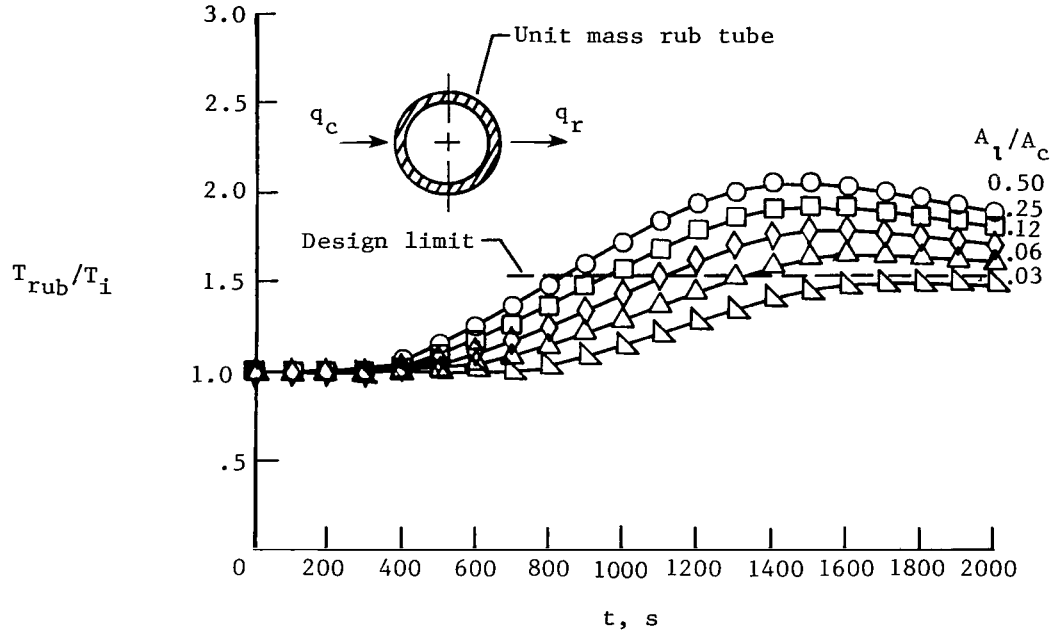

(a) T_i = 295 K.

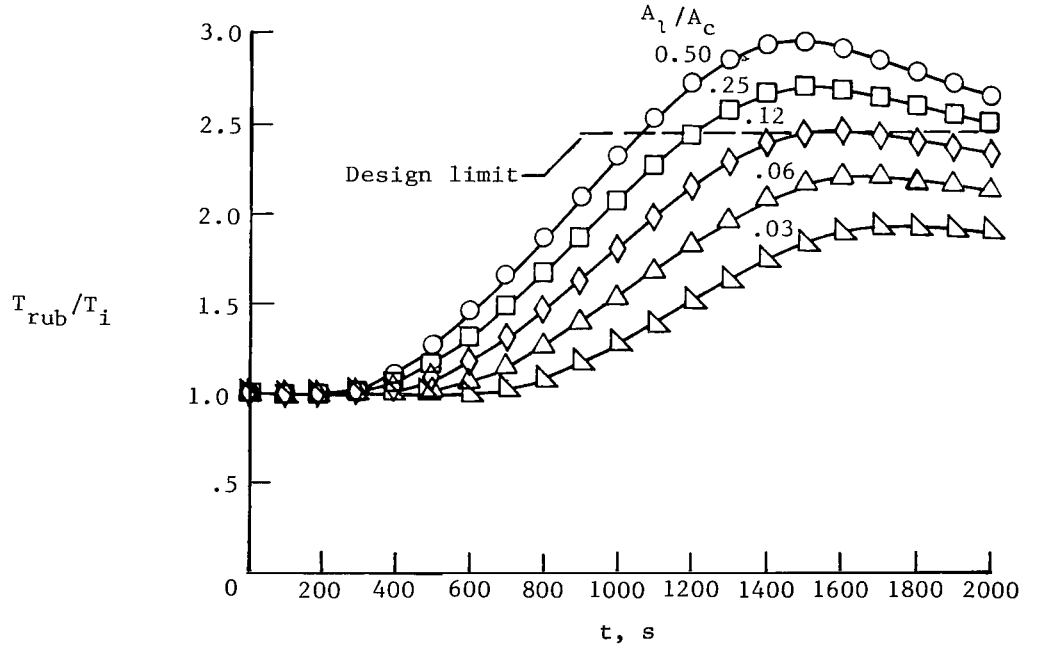

(b) T_i = 185 K.

Figure 21.- Rub-tube temperature histories for various leakage areas exposed to shuttle trajectory.

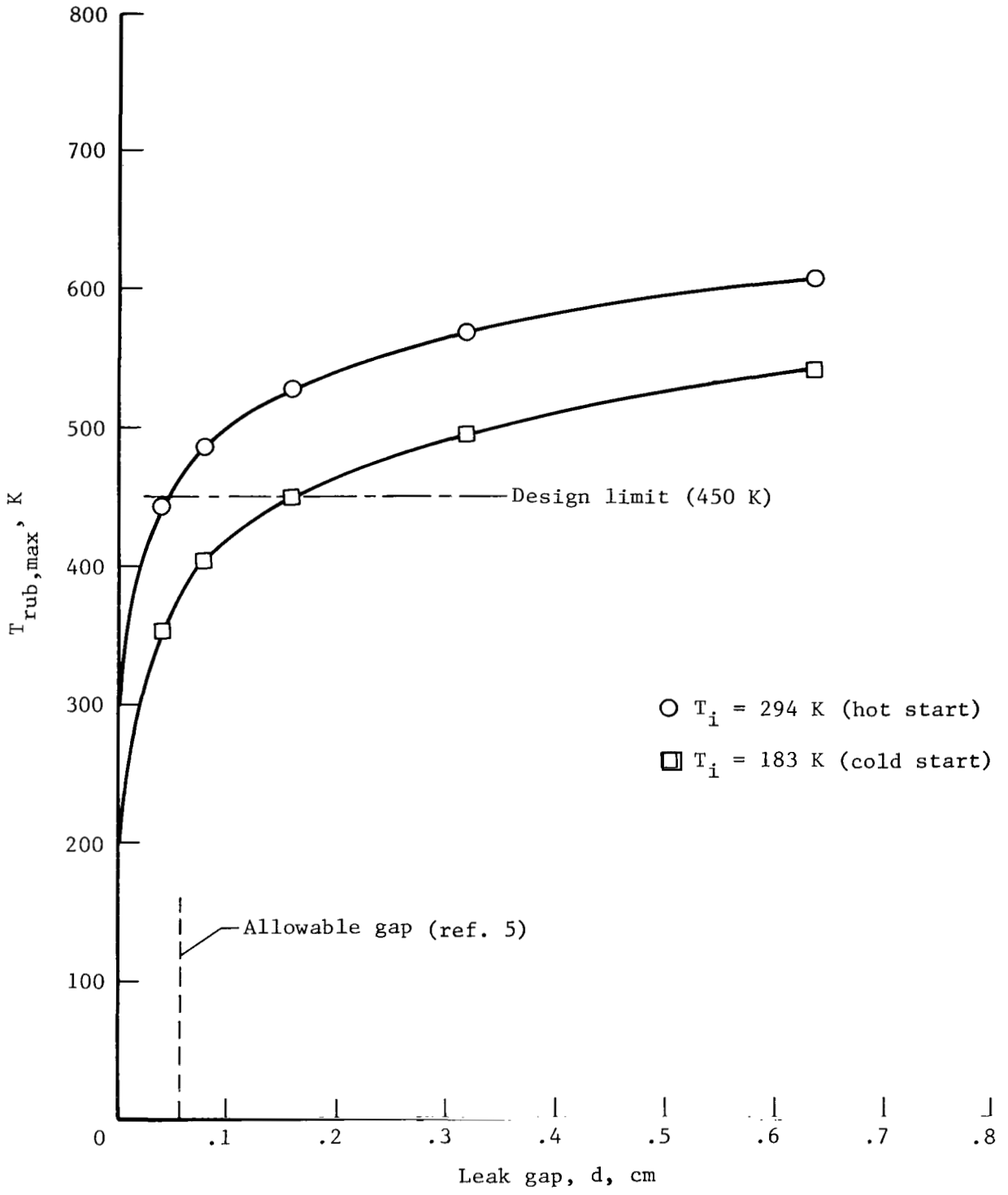

Figure 22.- Variation of maximum rub-tube temperature with leak gap.

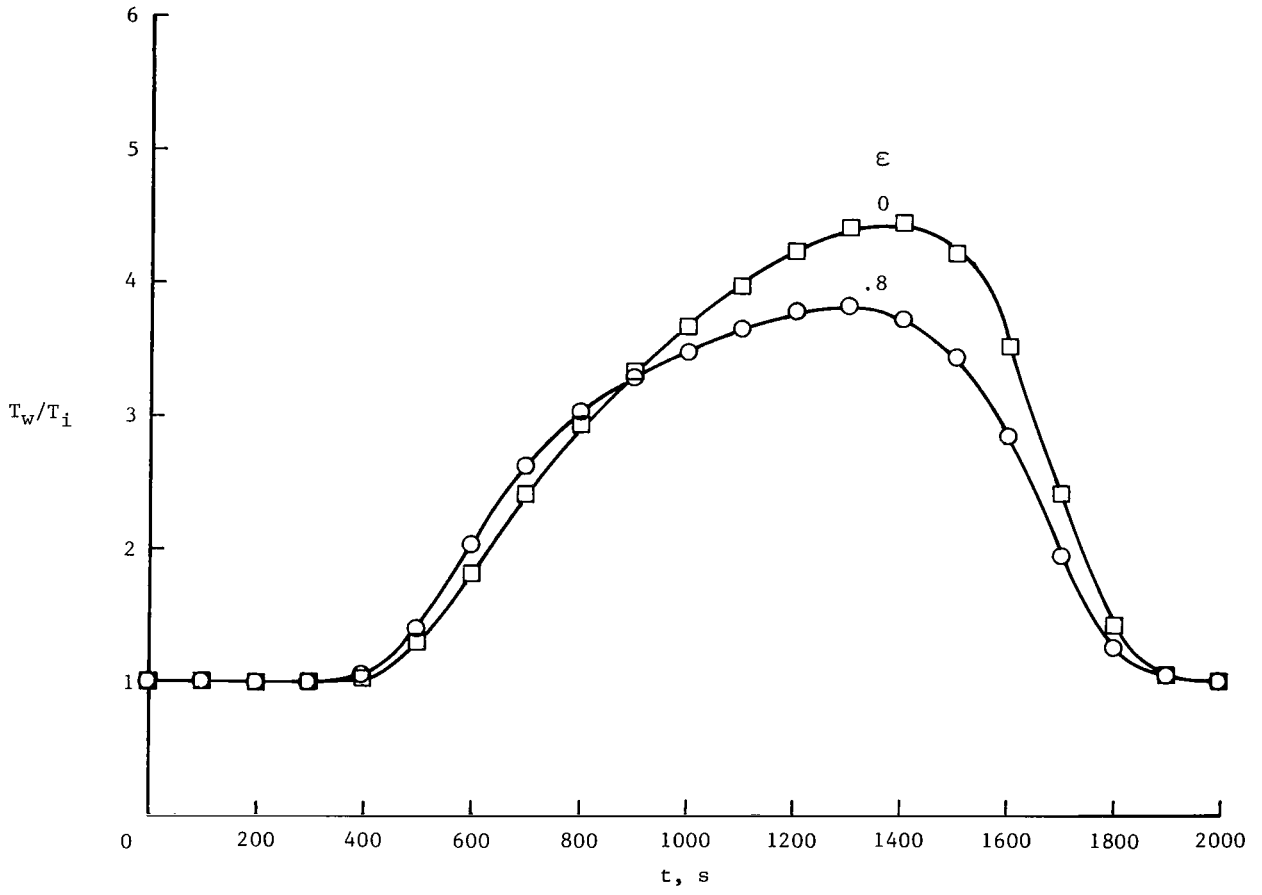

Figure 23.- Cove-exit wall-temperature histories for various surface emissivities exposed to a shuttle-entry condition. A_l/A_c = 0.06.

1. Report No.	2. Government Accession No.	3. Recipient's Catalog No.
NASA TP-1703		

4. Title and Subtitle

AEROTHERMAL ANALYSIS OF A WING-ELEVON COVE WITH VARIABLE LEAKAGE

5. Report Date: September 1980

6. Performing Organization Code:

7. Author(s)

L. Roane Hunt

8. Performing Organization Report No.: L-13751

10. Work Unit No.: 506-53-73-06

9. Performing Organization Name and Address

NASA Langley Research Center
Hampton, VA 23665

11. Contract or Grant No.:

13. Type of Report and Period Covered: Technical Paper

12. Sponsoring Agency Name and Address

National Aeronautics and Space Administration
Washington, DC 20546

14. Sponsoring Agency Code:

15. Supplementary Notes

16. Abstract

A mathematical model of the heating associated with leakage within the Space Shuttle Orbiter wing-elevon cove was used to analyze the aerothermal response of the structure. The analysis was applied to wind-tunnel results and to shuttle-entry conditions. A parametric study described the mechanism by which the energy of the ingested mass is distributed as a function of the Reynolds number, wall conductivity, surface emissivity, and cove height and length. In general, the rate at which energy was transferred into the cove interior was primarily determined by the combined effects of the convection, wall capacitance, and internal-radiation terms. Correlation with wind-tunnel results indicated that the cold-wall convective heating rates, wall temperature, and gas temperature of the cove were predicted by the analytical model for short exposure times. Predicted transient thermal response of the elevon cove subjected to shuttle-entry conditions indicated that the allowable leak area at the cove seal was 20 percent less than that previously indicated by experiment. To predict more accurate structural temperatures, the techniques used herein to represent the convective heat transfer must be incorporated into a more detailed structural model which would more accurately represent the cove geometry and thermal mass distribution.

17. Key Words (Suggested by Author(s))

Aerothermal analysis
Wing-elevon cove leakage
Heat-transfer distributions

18. Distribution Statement

Unclassified - Unlimited

Subject Category 34

19. Security Classif. (of this report)	20. Security Classif. (of this page)	21. No. of Pages	22. Price
Unclassified	Unclassified	41	A03

For sale by the National Technical Information Service, Springfield, Virginia 22161

NASA-Langley, 1980

2 1 1U,D, 090580 S00903DS
DEPT OF THE AIR FORCE
AF WEAPONS LABORATORY
ATTN: TECHNICAL LIBRARY (SUL)
KIRTLAND AFB NM 87117